Earth and Space Science

RESEARCH ARTICLE
10.1029/2019EA000645

Special Section:
Results from the Initial NASA Solar Irradiance Science Team (SIST) Program

Solar Irradiance Variability: Modeling the Measurements

J. L. Lean[1,2], O. Coddington[2], S. V. Marchenko[3], J. Machol[4], M. T. DeLand[3], and G. Kopp[2]

[1]Space Science Division, Naval Research Laboratory, Washington, DC, USA, [2]Laboratory for Atmospheric and Space Physics, University of Colorado Boulder, Boulder, CO, USA, [3]Science Systems and Applications, Inc., Lanham, MD, USA, [4]National Centers for Environmental Information, NOAA, Boulder, CO, USA

Abstract New models of the Sun's irradiance variability are developed from 15 years of direct observations made by the Solar Radiation and Climate Experiment (SORCE) spacecraft from 2003 to 2017 (inclusive). Multiple linear regression parameterizes the observations in terms of facular brightening and sunspot darkening, which are the primary sources of solar irradiance variability. The facular influence is specified as a combination of a linear and nonlinear solar ultraviolet (UV) index; the addition of the nonlinear term allows better reproduction of concurrent solar cycle and rotational variability. The sunspot darkening index is calculated using sunspot observations from both the Debrecen catalog and Air Force Solar Observing Optical Network (SOON) operational sites, the former providing superior model performance. The new model of total solar irradiance variability, NRLTSI3, with the Debrecen sunspot index reproduces the direct Total Irradiance Monitor (TIM) observations better than does the NRLTSI2 model that currently specifies irradiance for the NOAA Climate Data Record (CDR); the correlation of the model and observations increases from 0.956 to 0.971, and the standard deviation of the residuals decreases from 0.124 to 0.100 W m^{-2}. The new model of solar spectral irradiance variability, NRLSSI3, which extends from 115 to 100,000 nm, reproduces rotational modulation in independent Ozone Monitoring Instrument (OMI) observations at near-UV and visible wavelengths. The SATIRE model overestimates rotational modulation of near-UV Fraunhofer spectral features because of excess facular brightness; the EMPIRE model overestimates rotational modulation at all near-UV wavelengths.

Key Points:
- New models of solar irradiance variability, NRLTSI3 and NRLSSI3, are constructed from SORCE observations using improved facular and sunspot inputs
- OMI observations validate the new model during solar rotation; SATIRE and EMPIRE models overestimate this variability
- Faculae and sunspots may be less bright in the UV spectrum than SATIRE's theoretical stellar atmosphere model prescribes

Correspondence to:
J. L. Lean,
judith.lean.ctr@nrl.navy.mil

Citation:
Lean, J. L., Coddington, O., Marchenko, S. V., Machol, J., DeLand, M. T., & Kopp, G. (2020). Solar irradiance variability: Modeling the measurements. *Earth and Space Science*, *7*, e2019EA000645. https://doi.org/10.1029/2019EA000645

Received 26 MAR 2019
Accepted 10 MAY 2020
Accepted article online 18 MAY 2020

1. Introduction

Solar irradiance is Earth's dominant energy source and the only external agent of change of its surface and atmosphere. Consequently, the reliable specification of solar irradiance variability on multiple time scales informs a wide range of research and applications, the most obvious and controversial of which is the detection and attribution of the Sun's natural influence on climate (Gray et al., 2010; Lean, 2017; Matthes et al., 2017). The observational record of solar irradiance is one of 22 variables that NASA designates as crucial for Earth science, and it is an Essential Climate Variable (ECV) of the European Space Agency. In 2015 the National Oceanic and Atmospheric Administration (NOAA) implemented the Solar Irradiance Climate Data Record (CDR) to provide to the Earth science community operational estimates of solar total and spectral irradiance at wavelengths from 115 to 100,000 nm (Coddington et al., 2016).

Measurements made by dozens of radiometers on space-based platforms now span 40 years, contributing to long-duration observational databases of solar irradiance magnitude and variability that are essential for reliable climate change detection and attribution (NASEM, 2015). An outcome of ever lengthening solar irradiance databases and their ongoing scrutiny is the construction of composite observational records that combine multiple independent measurements with the goal of better characterizing solar irradiance cycles and detecting longer-term irradiance changes. Multiple composite records now exist of total solar irradiance since 1978 (e.g., Dewitte & Nevens, 2016; Dudok de Wit et al., 2017; Fröhlich & Lean, 2004). There are also a few composite records of solar spectral irradiance (DeLand & Cebula, 2008; Haberreiter et al., 2017) albeit with less fidelity because spectral irradiance observations are less accurate, exist primarily at ultraviolet (UV) wavelengths, and lack the overlap or the temporal repeatability necessary for straightforward cross-calibration.

In lieu of direct solar irradiance measurements (or composites thereof) with adequate duration and spectral coverage, Earth science research and applications such as the Climate Model Intercomparison Project (CMIP) and the Paleoclimate Model Intercomparison Project (PMIP), which simulate climate change for the Assessment Reports of the Intergovernmental Panel on Climate Change (IPCC), use as inputs the solar irradiance variability specified by models (Jungclaus et al., 2017; Matthes et al., 2017). Models of solar irradiance variability, constructed to reproduce contemporary observations, specify solar irradiance over the past one and a half millennia and across the entire electromagnetic spectrum. The Naval Research Laboratory Total Solar Irradiance (NRLTSI2) and Solar Spectral Irradiance (NRLSSI2) models parameterize irradiance observations in terms of indices of bright faculae and dark sunspots. The Spectral and Total Irradiance Reconstructions (SATIRE) uses a theoretical model of stellar atmospheres (Unruh et al., 2000) to specify the wavelength dependence of bright faculae and network and dark sunspot umbra and penumbra identified in solar magnetograms (Krivova et al., 2010, 2011). Additional models employ different numerical approaches, solar imagery, and theoretical models to quantify the influences of dark features associated with sunspots and bright features including faculae and network on solar irradiance variability (Ermolli et al., 2013).

Extant solar irradiance composites and models disagree about the temporal structure and wavelength dependence of the variability. For example, some composite reconstructions and the NRLTSI2 and NRLSSI2 models suggest modest changes in irradiance during consecutive solar minima during the past 40 years, whereas other composites and the SATIRE model suggest notable differences (Lean, 2017; Matthes et al., 2017); in the NRLTSI2 model the annual average value of total solar irradiance (TSI) in the 1986 solar minimum is comparable to that in the 2009 solar minimum (differing by 0.06 W m^{-2}), whereas in the SATIRE model it is 0.42 W m^{-2} higher. Since TSI in the cycle minimum in 2009 was 1.1 W m^{-2} less than during the solar cycle maximum in 2000, differences as large as 0.42 W m^{-2} in long-term trends inferred from cycle minima changes are a significant fraction (~40%) of the solar cycle amplitude. Spectral irradiance during the solar cycle varies ~50% less at wavelengths between 300 and 400 nm and more at visible and near-infrared wavelengths in the NRLSSI2 model than in the SATIRE model. Solar spectral irradiances between 300 and 1,000 nm contribute 68% of TSI and have similar temporal structure, so such wavelength-dependent differences affect the reconciliation of spectrally integrated variability with that of total irradiance.

As databases of solar irradiance observations continue to lengthen and advance, so too are extant models of solar irradiance variability tested and new models developed to reflect improved specification and emerging understanding. A component of NASA's Research Opportunities in Space and Earth Science (https://science.nasa.gov/blogs/roses-2014/2014/8/4/amendment-29-final-text-16-solar-irradiance-science-team), the Solar Irradiance Science Team (SIST), aims to provide reliable specification of solar irradiance variability for input to models of terrestrial variability so that the effects of variations in solar output can be properly represented and their impacts on the Earth system investigated. DeLand et al. (2019)summarize SIST activities which include the development of consistent multi-instrument space-based data sets of solar irradiance (both total and spectrally resolved) and comparisons of solar irradiance data sets with those of proxies to help define the range of relationships between them and support the inference of longer-term solar irradiance records to force the Earth system models.

This paper utilizes the most recent and reliable observations of solar irradiance and indices to advance, improve, and validate the performance of statistical models of solar irradiance variability, generating new models for eventual migration to a new version of NOAA's Solar Irradiance CDR. A companion paper (Coddington et al., 2019) demonstrates that the NOAA CDR, which uses the NRLTSI2 and NRLSSI2 models to specify solar irradiance (Coddington et al., 2016; Coddington & Lean, 2015), successfully reproduces total irradiance variations during the ~5 years subsequent to the 2003–2014 model "training period," thereby illustrating the stability and operational utility of such models. This motivates the systematic development, testing, and validation of new NRLTSI3 and NRLSSI3 models and their uncertainties, incorporating more recent irradiance observations and indices, for transition to future versions of the CDR in support of Earth science applications. Coddington et al. (2019) systematically compare the NRLTSI2 and NRLSSI2 models with the new models and with other models and measurements.

New proxy models of solar irradiance variability are constructed using measurements made by instruments on the Solar Radiation and Climate Experiment (SORCE) spacecraft (Rottman, 2005) from 2003 to 2017. A suite of statistical models of total solar irradiance variability is generated using the Total Irradiance Monitor (TIM) observations in combination with different facular and sunspot indices then evaluated to assess the preferred inputs. For comparison with the new NRLTSI3 model developed using the TIM observations, and to quantify uncertainties in the new model, separate models are also developed from six different composite records of observed TSI variations since 1978, including that developed as part of SIST. The facular and sunspot components of the new NRLTSI3 model constructed using the SORCE TIM observations are then used to construct a new, self-consistent model of spectral irradiance variability using observations made by SORCE's Spectral Irradiance Monitor (SIM) and Solar Stellar Irradiance Comparison Experiment (SOLSTICE).

Multiple statistical metrics are described to establish a methodology for quantifying the performance of new models of solar irradiance variability relative to extant models, thereby quantifying the extent to which they may, or may not, be applicable for transition to future versions of the NOAA CDR or for use in Earth science applications such as climate modeling and assessment. The metrics are evaluated to assess the performance of the new NRLTSI3 model developed from the SORCE TIM observations relative to multiple TSI composite records since 1978. Validation of the new NRLSSI3 model of spectral irradiance variability utilizes independent observations of spectral irradiance variability made by the Ozone Monitoring Instrument (OMI; Marchenko & DeLand, 2014; Marchenko et al., 2016), improved as part of SIST, and the new composite of Hydrogen I Lyman α emission at 121.5 nm developed as part of SIST (Machol et al., 2019). The comparisons of solar spectral irradiance variations observed by OMI with NRLSSI3, NRLSSI2, SATIRE, and EMPIRE (Yeo et al., 2017) models in the middle and near-UV spectrum articulate differences among the models that are traced to both their formulations and inputs.

2. Total Solar Irradiance

2.1. Measurements

Of all space-based solar irradiance measurements, those made by the TIM on SORCE (Kopp et al., 2005; Kopp & Lean, 2011) since 2003 have the smallest absolute uncertainty (±300 ppm) and the highest repeatability (±10 ppm per year). The TIM achieves high accuracy by judicious radiometer design, in which the defining aperture is positioned forward of the entrance baffle rather than of the entrance slit, and rigorous preflight calibration (Kopp et al., 2007). The high repeatability of its measurements is the result of in-flight sensitivity monitoring coupled with modest changes in cavity sensitivity (Kopp, 2014); the 200 ppm change in the sensitivity of TIM's primary cavity over 10 years is a factor of 5 or so smaller than calibration drifts in most other space-based solar radiometers over a similar period of time.

Since TIM observations commenced only in 2003, following the maximum of Solar Cycle 23, knowledge of total solar irradiance during previous cycles requires cross-calibration of TIM's absolute irradiance scale with that of radiometric measurements made prior to 2003, and corrections for their in-flight calibration drifts. The traditional approach combines judiciously selected data sets by cross calibration of their absolute scales and adjustment of their concurrent trends. The composite records of total solar irradiance constructed by the Physikalisch-Meteorologisches Observatorium Davos (PMOD; Fröhlich & Lean, 2004; Fröhlich, 2013), the Active Cavity Radiometer Irradiance Monitor (ACRIM; Willson, 2014; Scafetta & Willson, 2014), and the Royal Meteorological Institute of Belgium (RMIB; Dewitte & Nevens, 2016) are all products of this approach.

Differing from this traditional approach, three new TSI composite records are constructed by extracting from the measurements their common variability at different frequencies and combining these signals according to uncertainties of the individual measurements. Dudok de Wit et al. (2017) developed and applied this statistical approach to produce two different composite records of TSI variability as part of the European Solar Irradiance Data Exploitation (SOLID) initiative; one composite (SOLID) utilizes the TSI observations reported directly by the instrument teams, while a second composite (SOLID-C) corrects a subset of the measurements for "early signal increases" according to the prescription of Fröhlich (2006). A third such composite record of TSI observations is developed as part of the SIST effort.

Table 1
Web Locations and File Names of the Time Series of Solar Irradiance Observations, Models, and Indices Used in This Paper

Time series	Web location	File name
Total solar irradiance observations		
TIM	http://lasp.colorado.edu/home/sorce/data/tsi-data/#data_files	sorce_tsi_L3_c24h_latest.txt (181213)
PMOD	http://www-old.pmodwrc.ch/pmod.php?topic=tsi/composite/SolarConstant	composite_42_65_1709.dat (181213)
RMIB	ftp://gerb.oma.be/steven	TSI_composite_latest.txt (181213)
ACRIM	http://www.acrim.com/web30/ACRIM/data/default.html	composite_131130_hdr.txt
SOLID-C	https://projects.pmodwrc.ch/solid/index.php/main-database	TSI_composite.dat
SOLID	https://projects.pmodwrc.ch/solid/index.php/main-database	TSI_composite.dat
Solar spectral irradiance observations		
SORCE	http://lasp.colorado.edu/home/sorce/data/ssi-data/	sorce_ssi_L3_c24h_0000nm_2413nm_20030301_20181210.txt
OMI	https://sbuv2.gsfc.nasa.gov/solar/omi/	corrected_solar_flux_regular_diff_may_2018.sav
Facular and sunspot proxies		
Bremen Mg index	http://www.iup.uni-bremen.de/gome/gomemgii.html	MgII_composite.dat (181213)
SORCE Mg index	http://lasp.colorado.edu/lisird/	LISIRD_Mg_composite.txt (181219) sorce_mg_latest.txt (181213)
SOON sunspot regions	https://www.ngdc.noaa.gov/stp/space-weather/solar-data/solar-features/sunspot-regions/usaf_mwl/	multiple
Debrecen sunspot index	http://fenyi.solarobs.csfk.mta.hu/DPD/	debrecen_sunspot_blocking_corrected_heliographic_1975-01-01_2016-12-31.txt debrecen_sunspot_blocking_corrected_heliographic_2017-01-01_2017-12-31.txt
Balmaceda sunspot index	http://www2.mps.mpg.de/projects/sun-climate/data.html	sunspot_area_psi_20170531.txt
Solar irradiance variability models		
NOAA TSI CDR	https://www.ncei.noaa.gov/data/total-solar-irradiance/access/daily/	multiple
NOAA SSI CDR	https://www.ncei.noaa.gov/data/solar-spectral-irradiance/access/daily/	multiple
SATIRE TSI	http://www2.mps.mpg.de/projects/sun-climate/data.html	SATIRE-S_TSI_20180328.txt
SATIRE SSI	http://www2.mps.mpg.de/projects/sun-climate/data.html	SATIRE-S_20180328.sav
EMPIRE TSI	http://www2.mps.mpg.de/projects/sun-climate/data.html	EMPIRE_TSI_20170531.txt
EMPIRE SSI	http://www2.mps.mpg.de/projects/sun-climate/data.html	EMPIRE_SSI_20170531.txt

Table 1 lists the observation-based TSI records of the time series used in this paper and their web locations and file names.

2.2. Model Formulation

A model of TSI variability, $T_{mod}(t)$, seeks to replicate direct observations, $T_{obs}(t)$, at time t, in terms of known sources of irradiance variability, with minimum error in the residuals $R(t)$, where

$$T_{obs}(t) = T_{mod}(t) + R(t) \quad (1)$$

The primary sources of solar irradiance variability are bright faculae in compact plage and an extended network, and the central umbra and surrounding penumbra of dark sunspots. Solar irradiance varies because solar activity alters the occurrence of these magnetic features and hence their local emission relative to the Sun's "quiet" background emission. As these features erupt, evolve, and rotate on the solar hemisphere during the progression of the Sun's activity cycle, the projection at Earth of the altered local radiative output in faculae and sunspots respectively increases and decreases the Sun's irradiance.

The observed total solar irradiance, $T_{obs}(t)$, at time t may thus be modeled as a combination of facular and sunspot influences superimposed upon a "quiet" level;

$$T_{mod}(t) = T_Q \ + \Delta T_F(t) + \Delta T_S(t) \quad (2)$$

where T_Q is the baseline total solar irradiance and $\Delta T_F(t)$ and $\Delta T_S(t)$ are the amounts that faculae and sunspots, respectively, alter T_Q bolometrically (i.e., spectrally integrated). This approach adopts a constant value of T_Q in the space era because extant space-based TSI observations are insufficient for the reliable

detection of changes in the Sun's "quiet" irradiance level during the past 40 years. However, a variety of circumstantial evidence in historical proxies of solar activity suggests that the quiet Sun irradiance may not be invariant on multidecadal time scales (Lean et al., 2005; Wang et al., 2005).

Models of solar irradiance variability are readily constructed independently of direct space-based measurements by using ground-based solar observations that delineate the facular and sunspot sources and knowledge of their contrasts, either bolometric or at a particular wavelength. To demonstrate this, Lean et al. (1998) used histograms of solar images made in the Ca II k Fraunhofer line to quantify the total areas of bright regions, sunspot areas and locations determined from the Air Force Solar Observing Optical Network (SOON) white light images, and observation-based estimates of sunspot and facular contrasts. Their model successfully replicated independent observations of the Sun's total and UV spectral irradiance (at 200 nm) made by instruments on the Upper Atmosphere Research Satellite (UARS) during most of the declining phase of Solar Cycle 22, that is, from maximum to minimum solar activity. The model thus demonstrated that facular and sunspot magnetic sources fully account for both total and UV irradiance variations, thereby "obviating the need for an additional component other than spots or faculae" (Lean et al., 1998) during the contemporary epoch of space-based observations.

Models of solar irradiance variability may also be constructed by utilizing direct irradiance observations to establish the relative facular and sunspot contributions without the need for independent knowledge of their contrasts. The NRLTSI2 model, which NOAA uses to specify TSI for the CDR, calculates total solar irradiance, $T_{mod}(t)$, as

$$T_{\mathrm{mod}}(t) - T_Q = a_0 + a_1[M(t) - M_Q] + a_2 S(t) \tag{3}$$

with T_Q = 1,360.45 W m^{-2} and the three model coefficients, a_0, a_1, and a_2, determined by least squares regression of facular and sunspot indices against the SORCE TIM observations from 2003 to 2014 (Coddington et al., 2016; Lean et al., 2005). The ratio of space-based measurements of irradiance in the Mg II Fraunhofer line cores to that in the wings is the facular index, also known as the Mg II index, $M(t)$. The University of Bremen constructs a composite Mg index (for which M_Q = 0.15) by combining solar spectral irradiance observations made by the Global Ozone Monitoring Experiment (GOME), SCanning Imaging Absorption spectroMeter for Atmospheric CHartographY (SCIAMACHY), and GOME-2 instruments (Skupin et al., 2004; Snow et al., 2014). The index of the sunspot deficit is the sunspot darkening function, $S(t)$, calculated from direct observations of the area, A_s, and heliographic location, μ, of N_{spot} individual sunspots present on the solar disk at time t, allowing for the center-to-limb variation of the radiance, as (Foukal, 1981)

$$S(t) = 0.32 \sum_{i=1}^{N_{\mathrm{spot}}} A_{S_i} \left(\frac{3\mu_i + 2}{2} \right) \mu_i \tag{4}$$

The SOON sites measure the areas and locations of individual sunspot active regions present on the solar disk on any given day. Figure 1 shows the Bremen Mg index (Figure 1a) and the sunspot darkening index calculated from SOON operational sites (Figure 1c) from 1978 to 2017, and differences of these specific indices with other renditions. Figure 2 compares the NRLTSI2 TSI with the TIM observations (Figure 2a, left column) and shows the residuals, $R(t)$, of the observations and model (Figure 2b, left column) and their histogram distribution (Figure 2c, left column). Table 1 lists the solar irradiance variability models and facular and sunspot indices used in this paper, together with their web locations and filenames.

While the utility of the Mg II irradiance index for representing the facular contribution to solar irradiance variability is well established (DeLand & Cebula, 1993; Thuillier et al., 2012; Viereck et al., 2001, 2004), there is some uncertainty about whether the quantitative relationship is strictly linear, and the possible dependence of the relationship on wavelength and time. For example, Viereck et al. (2001) found a nonlinear relationship between the Mg index and the Solar Extreme Ultraviolet Monitor (SEM) irradiance at 30.4 nm. Fröhlich and Lean (2004) found that using a combination of daily and smoothed Mg indices increases the explained variance of the PMOD composite (from 1978 to 2004) from 77.2% to 78.6%. Woods et al. (2000) found that a model with both daily and smoothed Mg indices better reproduces solar Lyman α irradiance observations than a single Mg index.

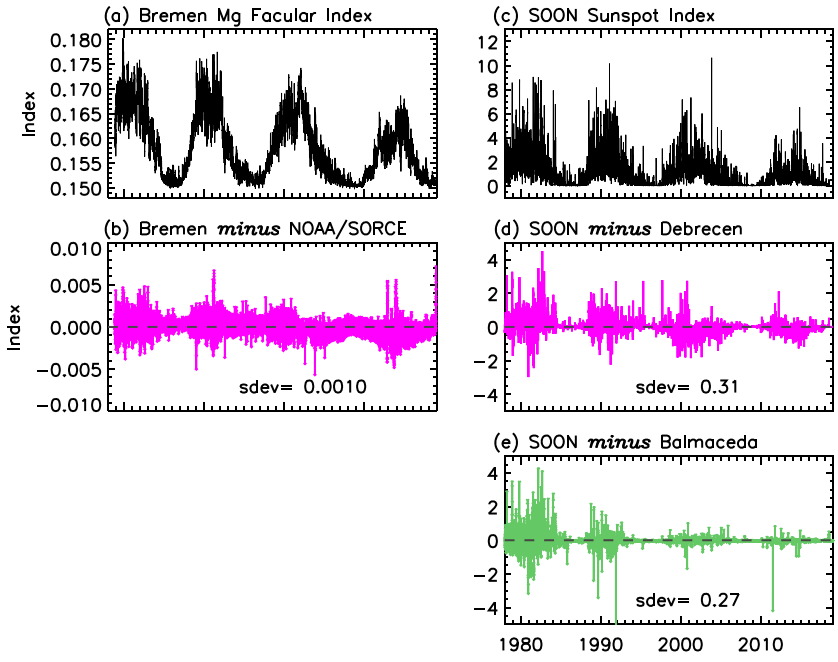

Figure 1. Compared are different facular and spot indices input to models of solar irradiance variability. (a) The Bremen Mg facular index and (b) the differences from this index of the (scaled) NOAA Mg index extended with the SORCE Mg index. (c) The sunspot darkening index constructed from SOON operational observations of sunspot areas and locations, (d) differences from the SOON sunspot index of a (scaled) index constructed from the Debrecen catalog of sunspot regions, and (e) differences from the SOON sunspot index of the (scaled) sunspot index constructed by Balmaceda et al. (2009).

Recognizing the potential for improved model performance using a nonlinear $M(t)$ dependence to provide an extra degree of freedom, a new statistical model of TSI variability, designated NRLTSI3, is formulated with two, rather than one, Mg index components, as

$$T_{\mathrm{mod}}(t) - T_Q = b_0 + b_1[M(t) - M_Q] + b_2[M(t) - M_Q]^x + b_3 S(t) \tag{5}$$

Linear regression against direct observations establishes the four model coefficients, b_0, b_1, b_2, and b_3, and their uncertainties for a specified value of the exponent, x. Since the TSI measurements and indices are specified relative to the quiet Sun, and since $S(t) = 0$ when $T_{mod} = T_Q$, then $b_0 \cong 0$. The bolometric irradiance change due to faculae is then

$$\Delta T_F(t) = b_1[M(t) - M_Q] + b_2[M(t) - M_Q]^x \tag{6}$$

and the bolometric irradiance change due to sunspots is

$$\Delta T_S(t) = b_3 S(t) \tag{7}$$

It is not possible to reliably isolate a single preferred value of the exponent, x, using existing TSI observations. When the model is constructed using the SORCE TIM observations with values of the exponent in the range $x = 0.95$ to $x = 1.5$, the model's b_1 and b_2 coefficients change, but the correlation of the model and observations and the standard deviation of the residuals remain stable to the third decimal place. Subsequent validation of the model's performance in section 2.5, using independent, longer-duration TSI composites, confirms the insensitivity of the model to the choice of the exponent in Equation 5 over a similar range.

To demonstrate the improvement of the new model formulation (Equation 5) relative to that of NRLTSI2 (Equation 3), Figure 2 (middle column) shows the new model constructed using the Bremen Mg facular index (with exponent $x = 0.96$, arbitrarily selected within the relevant range) and SOON sunspot index with TIM observations from 2003 to 2017. The correlation of this new model with the TIM observations is $r_2 = 0.965$ (for $n_2 = 5{,}463$ daily values with $df_2 = 1{,}309$ degrees of freedom), which is higher than the

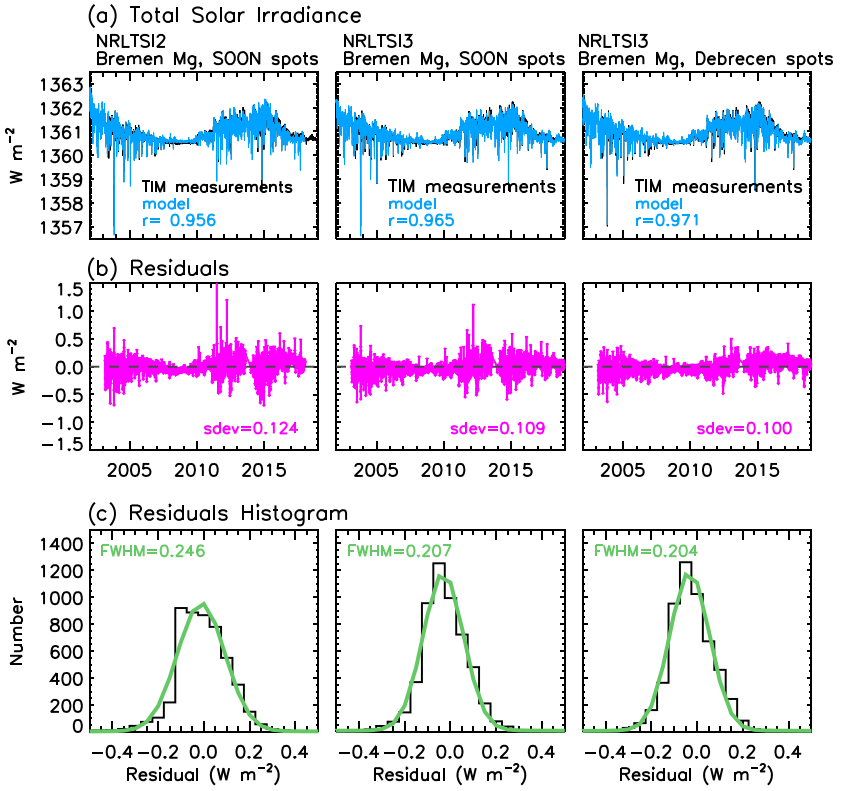

Figure 2. (a) Shown in each panel are the TIM measurements of total solar irradiance (black lines) compared with (left panel) the NRLTSI2 (NOAA CDR) model using the Bremen Mg index and the SOON sunspot index, (center panel) the NRLTSI3 model (Equation 5 with $x = 0.96$) also using the Bremen Mg index and the SOON sunspot index, and (right panel) the NRLTSI3 model using the Bremen Mg index and the Debrecen sunspot index. (b) The residuals of the TIM measurements and each of the three models and (c) the histograms of the residuals. The gap in the residuals near 2013 is due to the lack of TIM measurements. The green lines in (c) are Gaussian fits to the histograms of the residuals. The slight negative skew of the histogram peaks may reflect the tendency of the models to slightly overestimate the TIM measurements during solar cycle minima, evident in the slightly negative residual time series during 2008–2009, a tendency that is less pronounced in the NRLTSI3 model than in the NRLTS2 model. The middle panel quantifies the improvements in the NRLTSI3 model's representation of the TIM TSI observations relative to NRLTSI2, using the Bremen Mg facular index and SOON sunspot index in both models. The right panel quantifies the improvements in the NRLTSI3 model's representation of the observations using the Debrecen sunspot index instead of the SOON sunspot index (with the Bremen Mg facular index in both cases). From the left to right panels, the correlation coefficient increases, the standard deviation of the residuals of the model and observations decreases, and the histogram of the residuals narrows. The increase in the correlation coefficient, r, is a result of both an increase in the sum of squares of regression, $SSR = \sum_{i=1}^{n} (mod_i - obs_{av})^2$, which quantifies the strength of the linear relationship between the n values of the model, mod_i, and observations, obs_i, and a decrease in the sum of squares of the error, $SSE = \sum_{i=1}^{n} (mod_i - obs_i)^2$, which quantifies the spread of the model-observations residuals about the linear relationship. Specifically, $r^2 = \frac{SSR}{(SSR + SSE)}$; from left to right SSR increases from 857 to 867 to 875 and SSE decreases from 75 to 65 to 53.

correlation of the NRLTSI2 model with the TIM observations, for which $r_1 = 0.956$ (for $n_1 = 5{,}125$ daily values with $df_1 = 1{,}202$ degrees of freedom). The degrees of freedom, df, in the model is significantly less (by a factor of about 4) than the number of daily values, n, because of the presence of autocorrelation in the residuals of the model and observations. Assuming that the residuals may be approximated by a first-order autoregressive process, this is estimated as

$$df = \frac{(n - n_{\text{param}})}{[(1 + acf1)/(1 - acf1)]} \tag{8}$$

where $n_{\text{param}} = 4$ is the number of model parameters and $acf1$ is the autocorrelation of the residuals at a lag of 1 day.

The equivalent Fisher z transformation, $z = 0.5\,[ln(1+r) - ln(1-r)]$, of the correlation coefficient, r_1, of the NRLTSI2 model and the TIM observations is $z_1 = 1.9$; for the correlation, r_2, of the NRLTSI3 and the TIM observations it is $z_2 = 2.0$. The Z metric for the increase of a z score from $z_1 = 1.9$ to $z_2 = 2.0$, determined as

$$Z = \frac{(z_2 - z_1)}{\sqrt{\frac{1}{df_1 - 3} + \frac{1}{df_2 - 3}}} \tag{9}$$

is $Z = 2.5$. The cumulative standard normal distribution indicates that this Z value is significant at the 99.4% level. Even if the residuals are not exactly represented by a first-order autoregressive process and the degrees of freedom are an order of magnitude less than the number of observations (instead of a factor of 4), the corresponding $Z = 1.6$ indicates that the model improvement is still 94.5% significant.

Various additional metrics similarly confirm that the new model formulation (Equation 5) provides a better representation of the TIM observations than does the formulation used to construct NRLTSI2 (Equation 3). The standard deviation of the residuals, $R(t)$, of the model and observations, shown in Figure 2b, decreases from 0.124 to 0.109 W m^{-2}, the full width at half maximum of the histogram of the residuals, shown in Figure 2c, decreases from 0.246 to 0.207 W m^{-2}, and the peak of the histogram (which indicates the number of occurrences of residual values near 0) increases from ~900 to 1,140.

That the improvement in the model's specification of total solar irradiance variability with the addition of a nonlinear facular index term is practically 100% statistically significant is formally established using a metric, F_{add}, which is amenable to testing with the F probability distribution. Following Roscoe and Haigh (2007) and von Storch and Zwiers (1999)

$$F_{\text{add}} = df\left(\frac{SSR_{I+I_N} - SSR_I}{SSE_{I+I_N}}\right) \tag{10}$$

where $SSR = \sum_{i=1}^{n}(mod_i - obs_{av})^2$ is the sum of squares of regression and $SSE = \sum_{i=1}^{n}(mod_i - obs_i)^2$ is the sum of squares of the residuals of the model and observations; mod_i and obs_i are the n individual common values of the model and observations and obs_{av} is the mean of the observations. Specifically, SSR_{I+I_N} is the sum of squares and SSE_{I+I_N} the sum of squares of the residuals of the TSI variability model using both the daily and exponential Mg indices; SSR_I is the sum of squares of the model using just the daily Mg index. The number of degrees of freedom, df, takes into account autocorrelation of the residuals using Equation 8. Using the TIM observations, the Bremen Mg index, and the SOON sunspot darkening index from 2003 to 2017 to determine the model coefficients, $F_{\text{add}} = 200$ ($n = 5{,}463$, $df = 1{,}309$). According to the F probability distribution, values of $F_{\text{add}} > 10$ are >99% significant. Even if the number of degrees of freedom is an order of magnitude smaller than the number of observations, reducing F_{add} to 83, the addition of the nonlinear facular index term in the model is still practically 100% significant.

An alternative, more compact form of the NRLTSI3 model of total solar irradiance variability identifies the variations expressly in terms of the facular, $\Delta T_F(t)$, and sunspot, $\Delta T_S(t)$, components as

$$T_{\text{mod}}(t) - T_Q = c_0 + c_1\Delta T_F(t) + c_2\Delta T_S(t) \tag{11}$$

This specific formulation is used subsequently in section 2.3 to more efficiently estimate the uncertainties of the modeled irradiance and of the individual facular and sunspot components and in section 3 to construct corresponding models of spectral irradiance variability, NRLSSI3. For total solar irradiance variability, ΔT_F and ΔT_S are explicitly determined by Equations 6 and 7, so that in this case $c_0 = 0$, $c_1 = 1$, and $c_2 = -1$. These values of the coefficients are verified, and their uncertainties estimated by regressing the facular and sunspot irradiance components, instead of the indices themselves, against the TSI observations. For solar spectral irradiance variability c_1 and c_2 are no longer unity because the wavelength dependences of facular and sunspot contrasts means that their influences differ from their bolometric counterparts. The use of two inputs (i.e, ΔT_F and ΔT_S) instead of three (i.e., linear Mg, nonlinear Mg, and sunspot darkening indices) is essential when constructing the NRLSSI3 model because the lack of long-term repeatability of spectral irradiance

Table 2
Correlations of Observations and Models of TSI Variability Constructed From 42 Different Combinations of Observations and Facular and Sunspot Indices Using Equation 5 (With $x = 0.96$)

Mg index sunspot index	TSI TIM	TSI PMOD	TSI ACRIM	TSI RMIB	TSI SOLID-C	TSI SOLID	TSI SIST
Bremen SOON	**0.965** (1,309)	0.932 (2,898)	*0.826* (1,240)	0.931 (2,134)	0.918 (2,741)	*0.847* (1,341)	0.906 (2,994)
Bremen Debrecen	**0.971** (742)	0.940 (2,236)	*0.825* (1,016)	0.931 (1,358)	0.916 (1,889)	*0.842* (955)	0.906 (2,240)
Bremen Balmaceda	**0.961** (1,383)	0.927 (3,685)	*0.821* (1,400)	0.921 (2,719)	0.912 (3,358)	*0.836* (1,526)	0.900 (3,521)
NOAA/SORCE SOON	0.949 (1,505)	0.916 (2,416)	*0.817* (1,223)	0.923 (2,170)	0.909 (2,585)	*0.844* (1,363)	0.901 (2,916)
NOAA/SORCE Debrecen	**0.954** (1,168)	0.928 (2,085)	*0.819* (1,046)	0.928 (1,645)	0.912 (1,978)	*0.844* (1,030)	0.906 (2,392)
NOAA/SORCE Balmaceda	0.946 (1,554)	0.910 (2,944)	*0.811* (1,361)	0.914 (2,640)	0.903 (3,035)	*0.833* (1,617)	*0.895* (3,331)

Note. In parenthesis are the number of degrees of freedom, *df*, in the residuals of the observations and model. The two different facular indices are the Bremen and NOAA/SORCE Mg composite time series. The three different sunspot darkening indies are those constructed from SOON observations, the Debrecen Observatory catalog, and by Balmaceda et al. (2009). Correlation coefficients, *r*, greater than 0.95 are in bold; those less than 0.9 are in italics. The *z* transform of the correlation coefficient, $z = 0.5[\ln(1 + r) - \ln(1 - r)]$, for the TIM-Bremen-Debrecen combination is $z_1 = 2.0$ ($df_1 = 742$) and for PMOD-Bremen-Debrecen combination is $z_2 = 1.74$ ($df_2 = 2{,}236$). Therefore, $Z = (z_1 - z_2) \Big/ \sqrt{\frac{1}{df_1 - 3} + \frac{1}{df_2 - 3}} = 8.5$ for which the corresponding cumulative standard normal distribution indicates the difference in these two correlation coefficients is >99.9% significant.

observations precludes reliable model development using a formulation analogous to Equation 5 (i.e., with the additional facular index).

2.3. Model Inputs

The performance of a model of total solar irradiance variability depends on the fidelity of its facular and sunspot inputs. There are alternative realizations of the facular and sunspot indices to the Bremen Mg index and SOON sunspot darkening function used in the NRLTSI2 (CDR) and NRLTSI3 variability models shown in Figure 2 (left and middle columns, respectively). Figure 1b shows differences from the Bremen Mg index of another composite Mg index constructed from multiple NOAA/Solar Backscatter Ultraviolet (SBUV) measurements (Viereck et al., 2004), extended to the present with the SORCE/SOLSTICE Mg index (Snow et al., 2005). The absolute value of an Mg index depends on the instrument's spectral resolution; the NOAA/SORCE Mg index, for example, is about a factor of 2.5 less in magnitude than the Bremen Mg index and is linearly scaled prior to calculating the residuals in Figure 1b. Although not negligible, differences between these facular indices are small (~1%). Figures 1d and 1e show the differences from the SOON sunspot darkening index of the Debrecen (Győri et al., 2011) and Balmaceda et al. (2009) sunspot darkening indices, respectively. Differences during high solar activity are small (~1%) but larger (~10%) during solar minimum epochs when sunspot darkening approaches 0. For the period from 1978 to 2017 the standard deviations of the differences from the SOON index of the two indices are 31% and 27% of the mean value.

To assess whether the use of alternative indices improves the ability of the NRLTSI3 model to reproduce observed TSI variability, a suite of models is constructed using the TIM TSI observations with different facular and sunspot indices to determine model coefficients (Equation 5 with $x = 0.96$). Figure 2 (right column) illustrates the improvement in the NRLTSI3 model using the Debrecen instead of SOON sunspot darkening index (with the Bremen Mg index); the correlation of the model with TIM observations increases from 0.965 ($z = 2.0$) to 0.971 ($z = 2.1$), a change for which $Z = 2.17$, Equation 9, is >98% significant, the standard deviation of the residuals of the model and observations decreases from 0.109 to 0.10 W m^{-2}, and the full width at half maximum of the histogram of the residuals decreases from 0.207 to 0.204 W m^{-2}. Table 2 (second column) lists values of the correlations with observations of the models constructed using the TIM TSI observations and six different combinations of the Bremen and NOAA Mg indices and the SOON, Debrecen, and Balmaceda sunspot darkening indices. The improvement using the Debrecen instead of SOON (or Balmaceda) sunspot darkening index manifests when using the NOAA/SORCE Mg index as well as when using the Bremen Mg index.

To quantify the statistical significance of replacing an old index, $I_O(t)$, with a new index, $I_N(t)$, the metric F_{replace} is determined as

$$F_{\text{replace}} = df\left(\frac{SSR_{I_N} - SSR_{I_O}}{SSE_{I_N}}\right) \quad (12)$$

where SSR_{I_N} is the sum of squares of the TSI variability model, SSE_{I_N} is the sum of squares of the residuals using the new index, and SSR_{I_O} is the sum of squares of the TSI variability model using the old index. Replacing the SOON with the Debrecen sunspot darkening index, $F_{\text{replace}} = 103$, which indicates improved performance that is practically 100% significant. When replacing either the SOON or Debrecen sunspot darkening index with the Balmaceda et al. (2009) index, F_{replace} is negative and sufficiently large that it is practically 100% certain that the Balmaceda sunspot darkening index yields inferior performance when modeling TSI variability relative to both other sunspot darkening indices.

The observations of total solar irradiance made by TIM on SORCE, used to construct the NRLTSI2 and NRLTSI3 models shown in Figure 2, are acknowledged to have the highest repeatability of all space-based irradiance observations made thus far, but they commenced only in 2003 and thus extend for only 15 years. This raises the question of whether models of TSI variability constructed using longer composite records that now cover almost 40 years also show superior performance when formulated with the additional nonlinear facular index and the Debrecen sunspot index. To address this question, models of total solar irradiance variability are constructed using each of six different observational composite records (PMOD, ACRIM, RMIB, SOLID-C, SOLID, and SIST) with each of six combinations of the two facular and three sunspot darkening indices.

Compared in Figure 3 with the NRLTSI2 model from 1978 to 2017 (Figure 3, left column) is the new model constructed using Equation 5 (with $x = 0.96$) with the longer PMOD TSI composite record instead of the SORCE TIM observations and the Bremen Mg and SOON sunspot indices (Figure 3, middle column), and, separately, with the Bremen Mg and Debrecen sunspot indices (Figure 3, right column). Figure 3 also shows the residuals (Figure 3b) and the histogram distributions of the residuals (Figure 3c) corresponding to the different models/inputs. The comparisons of the TSI observations and models in Figure 3 confirm those in Figure 2, that using the additional nonlinear term and the Debrecen sunspot index increases the correlation with the measurements (from 0.929 to 0.940), decreases the standard deviation of the residuals of the model and observations (from 0.212 to 0.184 W m^{-2}), and decreases the full width at half maximum of the histogram of the residuals (from 0.302 to 0.280 W m^{-2}).

Table 2 (columns 3 to 8) lists values of the correlations with observations of the 36 additional models of TSI variability constructed using Equation 5 with each of the six different TSI composite observational records (in addition to the models constructed using the TIM observations, already described, in column 2) and multiple permutations of the Bremen and NOAA Mg indices and the SOON, Debrecen, and Balmaceda sunspot darkening indices. The highest correlation (0.94) among these 36 additional models pertains to that constructed with the PMOD irradiance composite, the Bremen Mg facular index, and the Debrecen sunspot darkening index. As with the models constructed using the TIM TSI, those constructed using all six TSI composites with either the NOAA/SORCE or Bremen Mg index have superior performance using the Debrecen and SOON sunspot darkening index instead of the Balmaceda sunspot index.

Of the total of 42 different realizations of the new model of TSI variability formulated using Equation 5 with different combinations of seven TSI observational records, two Mg indices, and three sunspot indices, that constructed by regressing the Bremen Mg index and the Debrecen sunspot darkening against the TIM observations is adopted as NRLTSI3 for subsequent comparisons in this paper with other models and observations and for the construction in section 3 of the corresponding spectral irradiance variability model, NRLSSI3. As the correlation coefficients in Table 2 indicate, and additional metrics confirm (e.g., Figures 2 and 3), this particular realization of the new model reproduces the observations used to determine the model coefficients better than does any of the models constructed using longer composite records (with any combination of facular and sunspot indices). For consistency with the NRLTSI2 and NRLSSI2 models, versions of the NRLTSI3 and NRLSSI3 models are also constructed using the Bremen Mg and the SOON sunspot darkening indices.

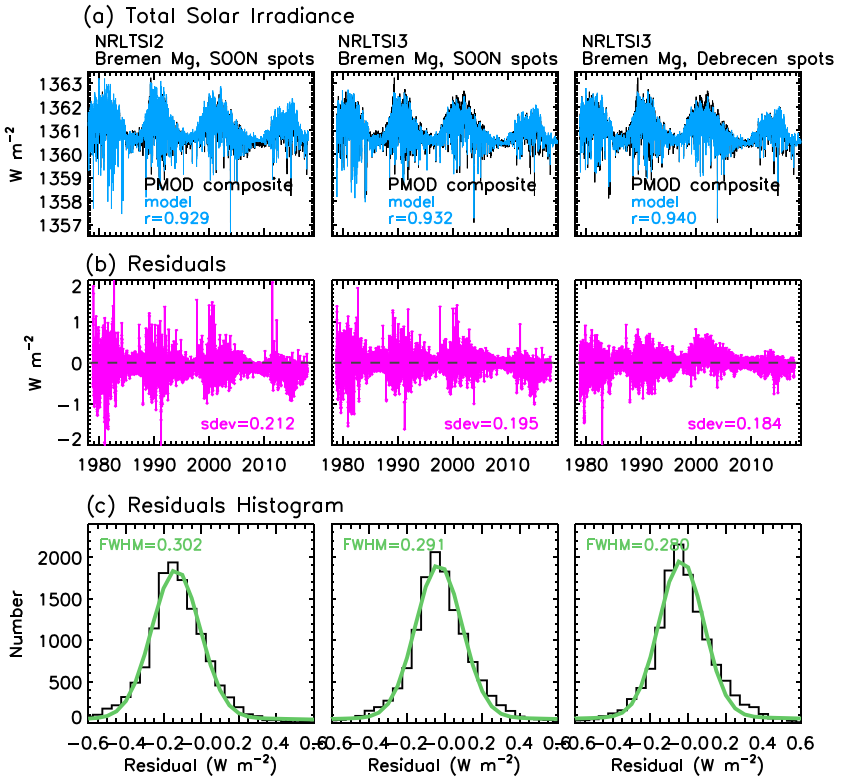

Figure 3. (a) Shown in each panel are the PMOD composite observations of total solar irradiance (black lines) compared with (left panel) the NRLTSI2 (NOAA CDR) model using the Bremen Mg index and the SOON sunspot index, (center panel) the NRLTSI3 model also using the Bremen Mg index and the SOON sunspot index, and (right panel) the NRLTSI3 model using the Bremen Mg index and the Debrecen sunspot index. (b) The residuals of the PMOD observations and each of the three models and (c) the histograms of the residuals. The green lines in (c) are Gaussian fits to the histograms of the residuals. The middle panel quantifies the improvements in the NRLTSI3 model's representation of the PMOD TSI observational composite relative to NRLTSI2, using the Bremen Mg facular index and SOON sunspot index in both models. The right panel quantifies the improvements in the NRLTSI3 model's representation of the observations using the Debrecen sunspot index instead of the SOON sunspot index (with the Bremen Mg facular index in both cases). From the left to right panels, the correlation coefficient increases, the standard deviation of the residuals of the model and observations decreases, and the histogram of the residuals narrows. The increase in the correlation coefficient, r, is a result of both an increase in the sum of squares of regression, $SSR=\sum_{i=1}^{n}(mod_i-obs_{av})^2$, which quantifies the strength of the linear relationship between the n values of the model, mod_i, and observations, obs_i, and a decrease in the sum of squares of the error, $SSE=\sum_{i=1}^{n}(mod_i-obs_i)^2$, which quantifies the spread of the model-observations residuals about the linear relationship. Specifically, $r^2=SSR/(SSR+SSE)$; from left to right SSR increases from 3,410 to 3,425 to 3,482, and SSE decreases from 530 to 515 to 457.

2.4. Model Uncertainties

The usual approach for estimating uncertainty in a model's determination of TSI is the propagation of errors in the model's inputs and coefficients. Since the NRLTSI3 model specifies total solar irradiance in terms of its quiet Sun value, T_Q, and its facular and sunspot components (Equation 11), model uncertainty is the quadrature sum of the uncertainties of these components;

$$\sigma_{\mathrm{mod}}(t)=\sqrt{\sigma_{\mathrm{quiet}}{}^2+(\sigma_{\mathrm{fac}}(t))^2+(\sigma_{\mathrm{spot}}(t))^2} \tag{13}$$

where

$$\sigma_{\mathrm{fac}}(t)=\sigma_{c_1\Delta T_F}(t)=c_1\Delta T_F(t)\sqrt{\left[\frac{\sigma_{c_1}}{c_1}\right]^2+\left[\frac{\sigma_{\Delta T_F(t)}}{\Delta T_F(t)}\right]^2} \tag{14}$$

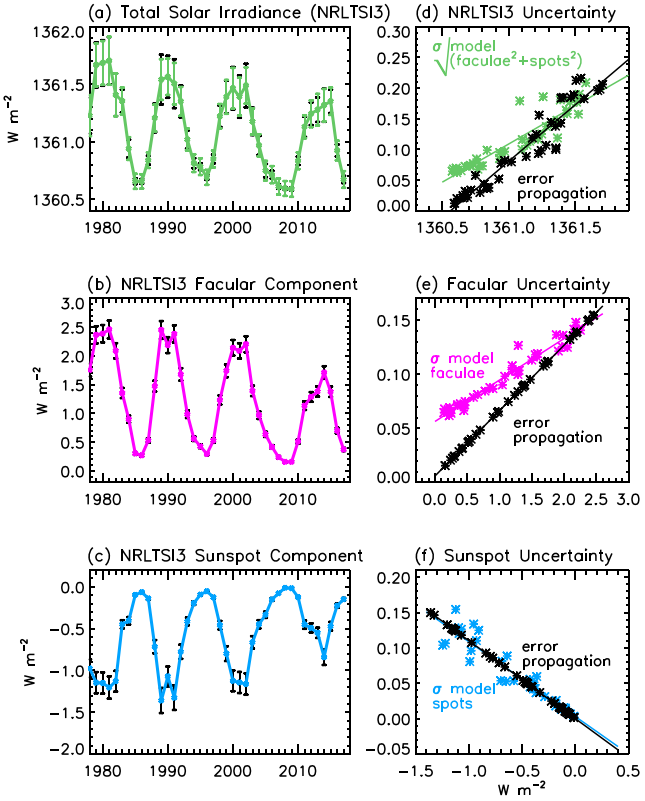

Figure 4. (a) Annual average values of total solar irradiance specified by the NRLTSI3 model since 1978 with estimated 1σ uncertainties. (b) The model's facular component and (c) the model's sunspot component, and their corresponding uncertainties. (d) The dependencies of the uncertainties in TSI on the TSI magnitude, determined by direct error propagation (black symbols) and from the standard deviations of the facular and sunspot components of models constructed using 42 different combinations of TSI observations and facular and sunspot indices (green symbols). (e) The dependencies of the uncertainties in the facular component on its magnitude and (f) the dependencies of the uncertainties in the sunspot component on its magnitude.

and

$$\sigma_{\text{spot}}(t) = \sigma_{c_2\Delta T_S}(t) = c_2\Delta T_S(t)\sqrt{\left[\frac{\sigma_{c_2}}{c_2}\right]^2 + \left[\frac{\sigma_{\Delta T_S(t)}}{\Delta T_S(t)}\right]^2} \quad (15)$$

since $c_0 \approx \sigma_{c_0} \approx 0$.

The uncertainties in the model's facular and sunspot components, $\sigma_{\text{fac}}(t)$ and $\sigma_{\text{spot}}(t)$, together quantify uncertainties in the variability of the modeled irradiance to which instrument calibration adds additional uncertainty, σ_{quiet}, in its absolute value. Estimating these uncertainties requires a priori knowledge of the uncertainties in the Mg II and sunspot darkening indices, which are not well specified. The propagation of errors used to estimate uncertainties in the NRLTSI2 model for the NOAA CDR assumed an uncertainty of ± 20% in the change of each of these indices from their solar minimum values.

An alternative approach for estimating uncertainties in $T_{\text{mod}}(t)$ makes use of the multiple models constructed using various combinations of the TSI observations and facular and sunspot indices; Table 2 identifies 42 such combinations pertaining to seven different TSI observational records (TIM, PMOD, ACRIM, RMIB, SOLID-C, SOLID, and SIST), two Mg facular indices (Bremen and NOAA/SORCE), and three sunspot darkening indices (SOON, Debrecen, and Balmaceda). The standard deviations of the facular and sunspot components of the 42 separate models provide independent estimates of the uncertainties of these components for use in Equation 13.

To illustrate estimates of the uncertainties in the NRLTSI3 model and its components, Figure 4a shows annual values of the modeled TSI with error bars (excluding σ_{quiet}) determined using two different approaches, specifically the direct propagation of uncertainties in the model coefficients and the facular and sunspot components (black symbols and lines) and, separately, as the standard deviation of the facular and sunspot components of the 42 separate models (colored symbols and lines). Figures 4b and 4c show the corresponding facular and sunspot components. Used for the propagation of errors (Equations 14 and 15) are $\frac{\sigma_{\Delta T_F(t)}}{\Delta T_F(t)} = 0.06$ and $\frac{\sigma_{\Delta T_S(t)}}{\Delta T_S(t)} = 0.11$ because these values provide approximate agreement with the uncertainties estimated independently by the standard deviations of the facular and sunspot components of the multiple models. The uncertainty in the facular and sunspot components, and hence in the change in TSI relative to its quiet value, depend on the magnitude of these components, being larger at times of higher solar activity. Figure 4d shows the dependence of uncertainties in TSI on the value of TSI itself (note that T_Q = 1360.45 W m^{-2}), Figure 4e shows the dependence of the uncertainties in the facular component on the value of the facular component itself, and Figure 4f shows the dependence of the uncertainties in the sunspot component on the value of the sunspot component itself.

The errors of the facular and sunspot components used to estimate the net uncertainties in the new NRLTSI3 model are those indicated by the linear dependence of the standard deviation of the multiple models' facular and sunspot components on the strength of these component, specifically, $\sigma_{T_F}(t) = 0.056 + 0.038\Delta T_F(t)$ (Figures 4e, pink line) and $\sigma_{T_S}(t) = 0.003 - 0.106(t)$ (Figures 4f, blue line). The errors are combined (in quadrature) to determine the uncertainty of the NRLTSI3 model of TSI variability for each day. As Figure 4d shows, the resultant uncertainties are of order 0.2 W m^{-2} at high solar activity and 0.05 W m^{-2} at low solar activity. The uncertainty in the annual modeled irradiance increase of ~1 W m^{-2} from solar cycle minimum to maximum, independent of the absolute scale uncertainty, is ~0.2 W m^{-2} (Figure 4d).

Finally, the additional absolute uncertainty in Equation 13 of $\sigma_{T_Q} = 0.9$ W m^{-2} is determined from the standard deviation of the seven TSI observational records each of which has its own calibration scale. The quadrature combination of uncertainties of the model's absolute scale ($\sigma_{T_Q} = 0.9$ W m^{-2}) and its average facular ($\sigma_{fac} \sim 0.1$ W m^{-2}) and sunspot ($\sigma_{spot} \sim 0.07$ W m^{-2}) components yields a representative $\sigma_{mod} \sim 0.91$ W m^{-2}.

2.5. Model Validation

Metrics determined in prior sections to quantify the agreement between models and the observations used to construct them establish that a statistical model of total solar irradiance variability that includes both linear and nonlinear facular terms (Equation 5) reproduces observed TSI variability better than does a model with a single linear facular term. This is true for both the TIM observations from 2003 to 2017 (Figure 1) and for the longer-duration PMOD composite from 1978 to 2017 (Figure 2). Since these metrics are calculated by comparing the model with the same observations used to estimate the model's coefficients, they measure the goodness of the model's fit to the observations but do not independently validate the model's ability to estimate TSI values not utilized for model construction.

Independent validation of the NRLTSI3 model performance requires additional metrics that compare the new model with observations not used to estimate the model coefficients. For this purpose, we statistically compare the TSI values estimated by the NRLTSI3 model constructed using the TIM observations from 2003 to 2017 and the Bremen Mg and Debrecen sunspot blocking indices with the PMOD, ACRIM, RMIB, SOLID-C, SOLID, and SIST composite time series. The PMOD, ACRIM, and RMIB composites are independent of the observations used to construct the model; they each employ the traditional approach of combining selected, cross-calibrated TSI data sets and do not include the TIM observations. While the SOLID, SOLID-C, and SIST composites, which are constructed by combining common variability at different frequencies in the measurements, do incorporate ~15 years of TIM observations since 2003, they are independent of TIM observations during the prior ~25 years.

Metrics of the performance of a model of TSI, T_{mod}, relative to n TSI observations, T_{obs}, include (von Storch & Zwiers, 1999; Wilks, 1995) the mean absolute error (MAE), root-mean-square error (RMSE), and mean absolute percentage error (MAPE). These quantities are determined numerically as

$$\mathrm{MAE} = \frac{1}{n}\sum_{k=1}^{n} |T_{\mathrm{mod}_k} - T_{\mathrm{obs}_k}| \tag{16}$$

$$\mathrm{RMSE} = \sqrt{\frac{1}{n}\sum_{k=1}^{n} (T_{\mathrm{mod}_k} - T_{\mathrm{obs}_k})^2} \tag{17}$$

$$\mathrm{MAPE} = \frac{100}{n}\sum_{k=1}^{n} \left(\frac{|T_{\mathrm{mod}_k} - T_{\mathrm{obs}_k}|}{T_{\mathrm{obs}_k}}\right) \tag{18}$$

where $T_{\mathrm{mod}} - T_{\mathrm{obs}}$ are the model-observation residuals, R (Equation 1).

Although the RMSE is widely used as a metric for assessing model performance, the MAE may be preferable for validating a model against observations. This is because the MAE simply averages the absolute model-observation residuals, whereas the RMSE depends not just on the magnitude of the residuals but also on "the distribution of error magnitudes (or squared errors) and $n^{1/2}$" (the square root of the number of residuals). For this reason, Willmott and Matsuura (2005) argue that average model performance is better assessed by the MAE rather than the RMSE, but Chai and Draxler (2014) question the superiority of MAE over RMSE, noting that combinations of metrics "are often required to assess model performance."

Table 3 therefore provides multiple metrics that quantify the performance of the NRLTSI3 model evaluated since 1978 against each of the six observational composites (none of which was used in the model's construction). In addition to the correlation coefficients of the NRLTSI3 model and observations, Table 3 lists numerical values for the MAE, RMSE, and MAPE of the residuals of the model and observations. For comparison, Table 3 also includes these same metrics for the NRLTSI2 and SATIRE models. Note that the models and observational composites each have their own absolute scales, differences of which do not affect the correlation coefficients but do affect the MAE, RMSE, and MAPE.

Table 3
Metrics Quantifying the Performance of the NRLTSI3 Model Constructed With the TIM TSI Observations From 2003 to 2017, the Bremen Mg Facular Index, and the Debrecen Sunspot Index, Using Equation 5.

Observations models	Number of days	Degrees of freedom	Correlation coefficient	Mean absolute error (W m^{-2})	Root-mean-square error (W m^{-2})	Mean absolute percentage error (%)
PMOD composite						
NRLTSI3 model	13,491	2,260	0.939	0.180	0.226	0.013
NRLTSI2 model	13,491	3,131	0.929	0.174	0.238	0.013
SATIRE model	13,491	2,050	0.909	0.212	0.294	0.016
RMIB composite						
NRLTSI3 model	12,080	1,353	0.929	2.284	2.292	0.168
NRLTSI2 model	12,080	2,267	0.927	2.288	2.297	0.168
SATIRE model	12,080	869	0.881	2.223	2.237	0.163
SOLID-C composite						
NRLTSI3 model	13,559	1,970	0.915	0.165	0.232	0.012
NRLTSI2 model	13,559	2,746	0.911	0.167	0.248	0.012
SATIRE model	13,559	1,542	0.858	0.216	0.316	0.016
SIST composite						
NRLTSI3 model	13,774	2,252	0.906	0.284	0.333	0.021
NRLTSI2 model	13,774	2,907	0.902	0.307	0.362	0.023
SATIRE model	13,774	1,704	0.846	0.289	0.339	0.021
SOLID composite						
NRLTSI3 model	13,559	999	0.841	0.231	0.344	0.017
NRLTSI2 model	13,559	1,519	0.842	0.228	0.345	0.017
SATIRE model	13,559	1,005	0.796	0.269	0.406	0.020
ACRIM composite						
NRLTSI3 model	12,043	1,028	0.820	0.375	0.462	0.028
NRLTSI2 model	12,043	1,388	0.819	0.382	0.480	0.028
SATIRE model	12,043	1,119	0.805	0.369	0.431	0.027
Average						
NRLTSI3 model			0.892	0.586	0.648	0.0430
NRLTSI2 model			0.888	0.591	0.662	0.0434
SATIRE model			0.849	0.596	0.671	0.0438
NRLTSI3 model						
$x = 0.5$			0.892	0.585	0.648	0.0430
$X = 0.67$			0.892	0.586	0.648	0.0430
$x = 0.9$			0.892	0.586	0.648	0.0431
$x = 0.96$ (above)			0.892	0.586	0.648	0.0430
$x = 1.1$			0.892	0.587	0.648	0.0431
$x = 1.4$			0.891	0.588	0.650	0.0432
$x = 1.5$			0.891	0.588	0.650	0.0432
$x = 2.0$			0.888	0.591	0.653	0.0434

Note. The metrics in the top six rows are determined from statistical comparisons of the new model with $x = 0.96$ (shown in Figure 2, right column) with six composites of TSI observations since 1978. Included are the correlation coefficients, mean absolute error (MAE), root-mean-square error (RMSE), and mean absolute percentage error (MAPE) of the models and observations. For comparison, the same performance metrics are determined for the NRLTSI2 and SATIRE models for days from 1978 to 2017 common in all three models. The bottom two rows list average values of the metrics for all six TSI composites, for the NRLTSI3, NRLTSI2, and SATIRE models, and for the NRLTSI3 model constructed using Equation 5 with different values of x.

Together, the metrics in Table 3 collectively establish that the new NRLTSI3 model constructed from 15 years of TIM observations reproduces independent TSI observations over the longer 40-year record better, on average, than does the NRLTSI2 model. The averages of the correlations of the NRLTSI3 and NRLTSI2 models with the six observational composites are 0.892 and 0.888, respectively, with the correlation of the NRLTSI3 model and observations exceeding that of the NRLTSI2 model and observations for five of the six observational composites. The average MAE, RMSE, and MAPE of the residuals of NRLTSI3 and the six composites are 0.586 W m^{-2}, 0.648 W m^{-2}, and .0430%, respectively, which are smaller than the corresponding averages for NRLTSI2 of 0.591 W m^{-2}, 0.662 W m^{-2}, and 0.0434%. The MAE, RMSE, and MAPE of the residuals of the NRLTSI3 model and observations is smaller than the corresponding metrics for the NRLTSI2 model-observations for a majority (respectively, four, six, and five) of the composites.

The metrics in Table 3 quantify the performance of the NRLTSI3 model constructed using Equation 5 with the particular exponent $x = 0.96$ by comparisons with six observational composite records of TSI variability over ~40 years. At the bottom of Table 3 are the average performance metrics of models constructed using Equation 5 with values of x ranging from $x = 0.5$ to $x = 2.0$. The model's performance is essentially unchanged for values of x in the range 0.5 to 1.1, confirming that $x = 0.96$ is an appropriate choice to illustrate the NRLTSI3 model formulation throughout this paper.

The NRLTSI3 and NRLTSI2-CDR models both perform better than the SATIRE model according to the metrics in Table 3 that compare these three models with six observational composites. The average correlation of the models and observations for both NRLTSI3 (0.892) and NRLTSI2 (0.888) exceed that for SATIRE (0.849). Also, the average MAE, RMSE, and MAPE of the residuals of the models and observations for both NRLTSI3 (0.586 W m^{-2}, 0.648 W m^{-2}, and 0.0430%) and NRLTSI2 (0.591 W m^{-2}, 0.662 W m^{-2}, and 0.0434%) are systematically smaller than the corresponding metrics for SATIRE (0.596 W m^{-2}, 0.671 W m^{-2}, and 0.0438%).

3. Solar Spectral Irradiance

3.1. Measurements

Multiple instruments have measured solar spectral irradiance at wavelengths shorter than 400 nm since 1980, including those on board the Solar Mesosphere Explorer (SME), UARS, and SORCE (Rottman, 2005, 2006; Rottman et al., 2005; Snow et al., 2010, 2018; Woods et al., 1996). Solar UV spectral irradiance is also a product of the SBUV instruments that measure primarily ozone concentrations on board multiple NASA and NOAA spacecraft (DeLand & Cebula, 1998). With the launch of SORCE in 2003 the database of solar spectral irradiance variability expanded to include visible and near-infrared wavelengths (Mauceri et al., 2018; Rottman et al., 2005; Woods et al., 2018). The SORCE spectral irradiance observations, which cover the wavelength range from 115 to 2,300 nm (Harder et al., 2010), have the longest duration (15 years) and broadest wavelength coverage of any spectral irradiance measurements thus far. Concurrent with SORCE measurements are those made by the OMI over a smaller wavelength interval from 265 to 500 nm (Marchenko & DeLand, 2014).

The lack of temporal overlap of the majority of solar spectral irradiance observations inhibits reliable cross calibration of their absolute scales. The construction of composite records therefore requires the use of proxy indicators or other techniques to interconnect independent observations (DeLand & Cebula, 2008; Haberreiter et al., 2017). Products of SIST include new spectral irradiance composites that include OMI measurements (DeLand et al., 2019; Marchenko et al., 2019) and a new composite record of HI Lyman α irradiance since 1947 (Machol et al., 2019) that combines the SORCE/SOLSTICE measurements with prior measurements made by spectroradiometers on the UARS, the SME, and Atmospheric Explorer E (AE-E) as well as modeled values based on the solar radio flux at 10.7 and 30 cm (F10.7 and F30) prior to 1978 and the Bremen Mg II index thereafter. This composite extends and improves the first such Lyman α composite of Woods et al. (2000).

3.2. Model Formulation and Inputs

A new statistical model of solar spectral irradiance variability, NRLSSI3, is constructed analogously to the NRLTSI3 model of total solar irradiance variability in section 2. The modeled spectral irradiance, $I_{\mathrm{mod}}(\lambda,t)$, at wavelength, λ, and time, t, is

$$I_{\mathrm{mod}}(\lambda, t) = I_Q(\lambda) + \Delta I_F(\lambda, t) + \Delta I_S(\lambda, t) \tag{19}$$

where $\Delta I_F(\lambda, t)$ and $\Delta I_S(\lambda, t)$ are the wavelength-dependent amounts that faculae and sunspots alter a reference solar irradiance spectrum, $I_Q(\lambda)$, such that $T_Q = \int_{\lambda_0}^{\lambda_\infty} I_Q(\lambda)\mathrm{d}\lambda$. As in NRLSSI2, the reference solar irradiance spectrum at wavelengths shorter than 2,400 nm is based on the absolute scale of the Whole Heliosphere Interval spectrum of Woods et al. (2009) but incorporating the somewhat higher spectral resolution of the SOLar SPECtrum (SOLSPEC) spectrum measured on the Atmospheric Laboratory of Applications and Science (ATLAS) 1 mission (Thuillier et al., 1998; Thuillier, private communication). At longer wavelengths, from 2,400 to 100,000 nm, the reference spectrum is based on a theoretical

stellar atmosphere model (Kurucz, 1991), adjusted to make the integrated energy of the quiet solar spectrum equal that of total solar irradiance.

While the fidelity of solar spectral irradiance observations continues to improve, at most wavelengths it is not yet possible to construct models of solar spectral irradiance variability using direct observations, $I_{obs}(\lambda, t)$, to establish the model coefficients because the magnitude of solar cycle variability is comparable to, or less than, that of the long-term repeatability of the observations. Possible exceptions are at far UV wavelengths less than 205 nm (DeLand & Cebula, 2012) and in strong solar transitions and line blends. An example is the dominant Hydrogen I Lyman α emission line at 121.6 nm for which the solar cycle change is ~50% and measurement repeatability ~5%.

Solar rotation also modulates spectral irradiance by altering the population of faculae and sunspots on the hemisphere of the Sun projected to Earth. The magnitude of this rotational modulation exceeds instrument sensitivity drifts over time scales of months. Therefore, to ameliorate contamination of modeled spectral irradiance variability by residual instrumental drifts in the observations, the NRLSSI3 model is constructed by first detrending the SORCE spectral irradiance measurements (by subtracting 81-day running means) then using linear regression to obtain initial estimates of the coefficients that quantitatively relate the detrended spectral irradiance changes with the similarly detrended bolometric facular and sunspot time series.

Use of the bolometric facular and sunspot components as the indices for the NRLSSI3 model recognizes that the integrals of the wavelength-dependent facular and sunspot components must equal the bolometric facular and sunspot components of total solar irradiance variability, so the facular and sunspot components at a given wavelength are proportional to their bolometric counterparts, that is, $\Delta I_F(\lambda, t) \propto \Delta T_F(t)$ and $\Delta I_S(\lambda, t) \propto \Delta T_S(t)$, where $\Delta T_F(t)$ and $\Delta T_S(t)$ are the time series determined using Equations 6 and 7 to transform the input Mg II and sunspot darkening indices. Explicitly, on time scales of solar rotation

$$I^{\text{rot}}_{\text{mod}}(\lambda, t) = d_0(\lambda) + d_1(\lambda)\left[\Delta T_F(t) - \langle \Delta T_F(t) \rangle_{81}\right] + d_2(\lambda)\left[\Delta T_S(t) - \langle \Delta T_S(t) \rangle_{81}\right] \tag{20}$$

where regression against the similarly detrended SORCE observations, $I_{\text{obs}}(\lambda, t) - \langle I_{\text{obs}}(\lambda, t) \rangle_{81}$ establishes the coefficients d_0, d_1, and d_2 at wavelength, λ.

To estimate solar spectral irradiance variations during the solar cycle using the coefficients derived from solar rotational modulation, the scaling of rotational to solar cycle variability is "calibrated" using TSI observations. This is necessary because the population of solar irradiance values that occurs during solar rotation does not encompass the full range possible during the solar cycle. Uncertainties in the irradiance observations and indices and limitations of the facular and sunspot proxy representations of irradiance variability cause the model coefficients derived from solar rotational modulation, alone, to differ slightly from those derived using directly observed rotational plus solar cycle changes. The model assumes that the facular and sunspot influences are linearly related to their respective disc-integrated bolometric counterparts at all wavelengths, differing only by a scaling coefficient. In reality the contrast of an individual bright active region or network element or of a sunspot's dark umbra or penumbra may depend on its heliographic location, differing from that of the disc-integrated Mg emission that forms the Mg index or from the bolometric sunspot darkening function in different ways at different wavelengths. Furthermore, the nonlinear Mg term used to construct the bolometric facular index may not be optimal for separate active regions and network, nor for individual wavelengths.

To quantify the scaling of solar rotational to solar cycle variability the coefficients that relate the similarly detrended TSI observations (i.e., with 81-day running means removed) to the detrended facular and sunspot time series are compared with those determined using the direct (i.e., not detrended) TSI observations. The model of TSI variability determined from rotational modulation is

$$T^{\text{rot}}_{\text{mod}}(t) = e_0 + e_1\left[\Delta T_F(t) - \langle \Delta T_F(t) \rangle_{81}\right] + e_2\left[\Delta T_S(t) - \langle \Delta T_S(t) \rangle_{81}\right] \tag{21}$$

where regression against the similarly detrended SORCE TSI observations, $T_{\text{obs}}(\lambda, t) - \langle T_{\text{obs}}(\lambda, t) \rangle_{81}$, determines the coefficients e_0, e_1, and e_2. An initial model of spectral irradiance variability due to facular and sunspot changes during the solar cycle is then

$$I_{\mathrm{mod}}(\lambda,t)-I_Q(\lambda)=d_0(\lambda)+d_1(\lambda)\left[\frac{c_1}{e_1}\right]\Delta T_F(t)+d_2(\lambda)\left[\frac{c_2}{e_2}\right]\Delta T_S(t) \tag{22}$$

where c_1 and c_2 are the coefficients of the NRLTSI3 model (Equation 9) and the ratios $\frac{c_1}{e_1}$ and $\frac{c_2}{e_2}$ scale the coefficients determined for spectral irradiance rotational modulation (Equation 20). It may be expected that in the ideal case where the facular and sunspot indices exactly represent the irradiance changes accruing from these respective variability sources, and for noise-free time series of observations and indices, the ratios $\frac{c_1}{e_1}$ and $\frac{c_2}{e_2}$ are unity. When determined using the TIM TSI observations, the Bremen Mg index to specify bolometric faculae and the Debrecen database to specify bolometric sunspot darkening, these scaling factors are $\frac{c_1}{e_1}=1.2$ and $\frac{c_2}{e_2}=1.05$. Since the SORCE spectral irradiance observations extend only to ~2,300 nm, model coefficients at the longer wavelengths from 2,300 to 100,000 nm are estimated using theoretical stellar atmosphere models of facular and sunspot contrasts (Unruh, private communication, April 2018).

A quantitative assessment of the fidelity of the initial model of solar spectral irradiance variability according to Equation 22 is the extent to which the integrals of the spectral facular and sunspot components agree with their respective bolometric counterparts. Since numerically, the integral of solar spectral irradiance at any time must equal the total solar irradiance at that time, $T_{mod}(t)=\int_{\lambda_0}^{\lambda_\infty} I_{mod}(\lambda,t)d\lambda$, so too must $\Delta T_F(t)=\int_{\lambda_0}^{\lambda_\infty}\Delta I_F(\lambda,t)d\lambda$ and $\Delta T_S(t)=\int_{\lambda_0}^{\lambda_\infty}\Delta I_S(\lambda,t)d\lambda$. The final step in the construction of the NRLSSI3 spectral irradiance variability model ensures these equivalencies. The differences between the bolometric facular and sunspot components of NRLTSI3 determined from the TIM TSI observations by Equation 11 and the spectrally integrated facular and sunspot components determined from SORCE spectral irradiance observations by Equation 22 are

$$\Delta T_F^{\mathrm{dif}}(t)=\Delta T_F(t)-\textstyle\int_{\lambda_0}^{\lambda_\infty}\Delta I_F(\lambda,t)\mathrm{d}\lambda \tag{23}$$

and

$$\Delta T_S^{\mathrm{dif}}(t)=\Delta T_S(t)-\textstyle\int_{\lambda_0}^{\lambda_\infty}\Delta I_S(\lambda,t)\mathrm{d}\lambda \tag{24}$$

where $\Delta I_F(\lambda,t)=d_1(\lambda)\left[\frac{c_1}{e_1}\right]\Delta T_F(t)$ and $\Delta I_s(\lambda,t)=d_2(\lambda)\left[\frac{c_2}{e_2}\right]\Delta T_S(t.)$ Were the initial NRLSSI3 model a "perfect" representation of the solar spectral irradiance variability that accounts for NRLTSI3 variability, the differences $\Delta T_F^{\mathrm{dif}}(t)$ and $\Delta T_S^{\mathrm{dif}}(t)$ would be 0 at all times, t. However, the actual numerical values of the differences, although small, are nonnegligible and depend on solar activity, being larger for higher values of the facular and sunspot components. These relationships are established numerically as $\Delta T_F^{\mathrm{dif}}(t)=f_0+f_1\Delta T_F(t)$ and $\Delta T_S^{\mathrm{dif}}(t)=g_0+g_1\Delta T_S(t)$. When using the Bremen Mg index, Debrecen sunspot darkening and TIM TSI observations in the construction of the NRLSSI3 model, the coefficients are f_0 ~ 0, $f_1=0.02$, g_0 ~ 0, and $g_1=-0.04$. $\Delta T_F^{\mathrm{dif}}$ and ΔT_F are highly correlated (correlation coefficient of 1) since they are both functions of the facular index; similarly, $\Delta T_S^{\mathrm{dif}}$ and ΔT_S are highly correlated since they are both functions of the sunspot darkening index.

Incorporating these adjustments to ensure that the integral of the modeled spectral irradiance numerically equals the modeled total solar irradiance at all times, the NRLSSI3 statistical model of spectral irradiance variability at a particular wavelength, λ, is then

$$I_{\mathrm{mod}}(\lambda,t)-I_Q(\lambda)=d_0(\lambda)+d_1(\lambda)\left[\frac{c_1}{e_1}\right]\left(\Delta T_F(t)+\Delta T_F^{\mathrm{dif}}(t)\right)+d_2(\lambda)\left[\frac{c_2}{e_2}\right]\left(\Delta T_S(t)+\Delta T_S^{\mathrm{dif}}(t)\right) \tag{25}$$

where $d_0(\lambda)\approx 0$. In terms of Equation 19, the facular and sunspot influences on spectral irradiance are specifically

$$\Delta I_F(\lambda,t)=d_1(\lambda)\left[\frac{c_1}{e_1}\right]\left(\Delta T_F(t)+\Delta T_F^{\mathrm{dif}}(t)\right)=d_1(\lambda)\left[\frac{c_1}{e_1}\right]\Delta T_F(t)+d_1(\lambda)\left[\frac{c_1}{e_1}\right]f_1\,\Delta T_F(t) \tag{26}$$

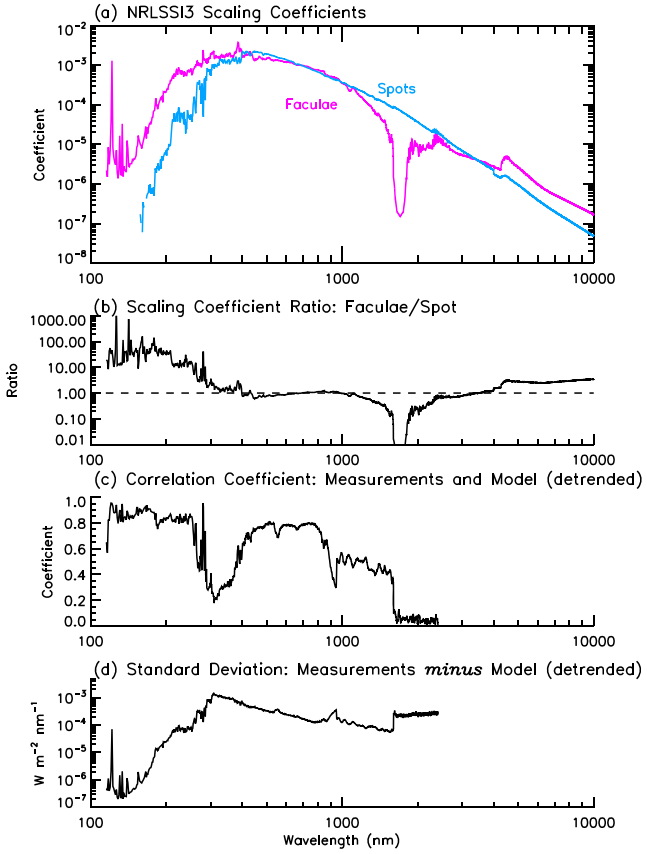

Figure 5. Parameters and metrics of the NRLSSI3 model constructed from detrended SORCE observations. (a) The model coefficients that scale the bolometric facular (magenta) and sunspot (blue) time series to determine the corresponding spectral irradiance changes at a given wavelength. (b) The ratios of the scaling coefficients indicate the relative importance of faculae versus sunspots for spectral irradiance variability at a given wavelength. (c) The correlation coefficients of the detrended SORCE measurements and NRLSSI3 model and (d) the standard deviations of the detrended SORCE measurements and NRLSSI3 model.

and

$$\Delta I_S(\lambda,t) = d_2(\lambda)\left[\frac{c_2}{e_2}\right]\left(\Delta T_S(t) + \Delta T_S^{\mathrm{dif}}(t)\right) = d_2(\lambda)\left[\frac{c_2}{e_2}\right]\Delta T_S(t) + d_2(\lambda)\left[\frac{c_2}{e_2}\right] g_1 \Delta T_S(t) \quad (27)$$

Figure 5a shows the spectral dependence of the NRLSSI3 model coefficients for the facular and sunspot components and Figure 5b shows the ratios of these coefficients, which characterize the relative contributions of faculae and sunspots to spectral irradiance variability at different wavelengths. In Figures 5c and 5d are metrics quantifying the regression model. The relatively low correlation coefficients of the model and observations (Figure 5c) and relatively high standard deviations of the residuals (Figure 5d) in the wavelength region 300 to 400 nm reflect the transition of the SORCE observations from measurements made by SOLSTICE to those made by SIM, whose signal-to-noise ratio is smaller at near UV and near-infrared wavelengths. The very low correlation coefficients of the model and observations at wavelengths longer than 1,600 nm indicates that the facular and sunspot influences on irradiance variability are barely detectable from noise in the SIM observations at wavelengths from 1,600 to 2,400 nm.

As the facular and sunspot influences increase from the minimum to the maximum of the solar cycle, the solar spectral irradiance changes accordingly. Figure 6 shows the spectrum changes from cycle minimum to maximum during Solar Cycle 23 (left column) and Cycle 24 (right column) that the NRLSSI3 model estimates, compared with the NRLSSI2 (CDR) and two other models. It can be seen in Figure 6a that the variability during Solar Cycle 24 (right column of Figure 6) at near-UV wavelengths from 300 to 400 nm is larger in NRLSSI3 (0.206 W m^{-2}) than in NRLSSI2 (0.181 W m^{-2}). Nevertheless, the Solar Cycle 24 increases in both models are smaller than in the SATIRE model (0.226 W m^{-2}), especially at wavelengths of Fraunhofer lines, and the EMPIRE model (0.280 W m^{-2}) at all wavelengths. Figure 6b shows the spectral irradiance energy changes at wavelengths from 100 to 10,000 nm and Figure 6c shows these changes as percentage increases. The slightly larger Solar Cycle 24 increase in the new NRLSSI3 model relative to NRLSSI2 is evident also at visible wavelengths, reflecting slightly larger TSI variability in the new model; the Cycle 24 increase at wavelengths from 500 to 750 nm is 0.258 W m^{-2} in NRLSSI3 and 0.222 W m^{-2} in NRLSSI2, with both models having larger visible irradiance increases than the SATIRE (0.157 W m^{-2}) and EMPIRE (0.191 W m^{-2}) models. Differences in solar cycle changes estimated by the NRLSSI3 and NRLSSI2 models at infrared wavelengths reflect different incorporations of theoretical facular contrasts, which extant observations cannot yet verify. Coddington et al. (2019) discuss in more detail the differences among the various models, including the discrepancies between the EMPIRE and SATIRE models that contradict their purported agreement (Yeo et al., 2017).

3.3. Model Uncertainties

The uncertainty in the NRLSSI3 model of spectral irradiance variability at a specific wavelength and time is obtained by propagating the uncertainties in the facular and sunspot components and the model coefficients, that is,

$$\sigma_{\mathrm{mod}}(\lambda,t) = \sqrt{\sigma_{\mathrm{quiet}}(\lambda)^2 + \left(\sigma_{\mathrm{fac}}(\lambda,t)\right)^2 + \left(\sigma_{\mathrm{spot}}(\lambda,t)\right)^2} \quad (28)$$

where $\sigma_{\mathrm{fac}}(\lambda,t) = \sigma_{\Delta I_F(\lambda,t)}$ (Equation 26) and $\sigma_{\mathrm{spot}}(\lambda,t) = \sigma_{\Delta I_S(\lambda,t)}$ (Equation 27). The uncertainties at wavelength, λ, and time, t, are thus

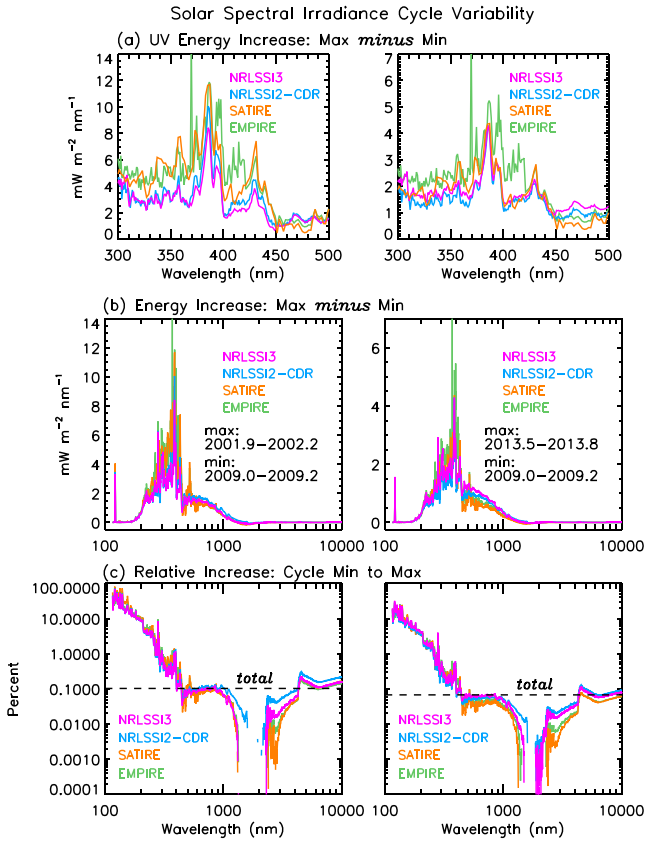

Figure 6. Changes in solar spectral irradiance during the solar cycle according to the NRLSSI3 model (magenta), the NRLSSI2 model (blue), and the SATIRE (orange) and EMPIRE (green) models. On the left are the changes during Solar Cycle 23, and on the right during Solar Cycle 24. (a) Spectral energy increases at wavelengths between 300 and 500 nm, from solar cycle minimum (2009.0–2009.2) to solar cycle maximum (2001.9–2002.2 in Cycle 23 and 2013.5–2013.8 in Cycle 24). (b) The spectral energy increases over a wider wavelength range, from 100–10,000 nm, and (c) the corresponding relative increases in percentages.

$$\left(\sigma_{\Delta I_F(\lambda,t)}\right)^2 = \left(d_1(\lambda)\left[\frac{c_1}{e_1}\right]\Delta T_F(t)\right)^2\left[\left(\frac{\sigma_{d_1}}{d_1}\right)^2 + \left(\frac{\sigma_{c_1}}{c_1}\right)^2 + \left(\frac{\sigma_{e_1}}{e_1}\right)^2 + \left(\frac{\sigma_{\Delta T_F(t)}}{\Delta T_F(t)}\right)^2\right] + \left(d_1(\lambda)\left[\frac{c_1}{e_1}\right]f_1\Delta T_F(t)\right)^2\left[\left(\frac{\sigma_{d_1}}{d_1}\right)^2 + \left(\frac{\sigma_{c_1}}{c_1}\right)^2 + \left(\frac{\sigma_{e_1}}{e_1}\right)^2 + \left(\frac{\sigma_{f_1}}{f_1}\right)^2 + \left(\frac{\sigma_{\Delta T_F(t)}}{\Delta T_F(t)}\right)\right] \quad (29)$$

and

$$\left(\sigma_{\Delta I_S(\lambda,t)}\right)^2 = \left(d_2(\lambda)\left[\frac{c_2}{e_2}\right]\Delta T_S(t)\right)^2\left[\left(\frac{\sigma_{d_2}}{d_2}\right)^2 + \left(\frac{\sigma_{c_2}}{c_2}\right)^2 + \left(\frac{\sigma_{e_2}}{e_2}\right)^2 + \left(\frac{\sigma_{\Delta T_S(t)}}{\Delta T_S(t)}\right)^2\right] + \left(d_2(\lambda)\left[\frac{c_2}{e_2}\right]g_1\Delta T_S(t)\right)^2\left[\left(\frac{\sigma_{d_2}}{d_2}\right)^2 + \left(\frac{\sigma_{c_2}}{c_2}\right)^2 + \left(\frac{\sigma_{e_2}}{e_2}\right)^2 + \left(\frac{\sigma_{g_1}}{g_1}\right)^2 + \left(\frac{\sigma_{\Delta T_S(t)}}{\Delta T_S(t)}\right)\right] \quad (30)$$

The uncertainties in the bolometric faculae and sunspot darkening are $\sigma_{\Delta T_F}(t) = 0.056 + 0.038\Delta_F(t)$, and $\sigma_{\Delta T_S}(t) = 0.003 - 0.106\Delta_S(t)$, determined in section 2 (Figure 4e, pink line and 4f, blue line) as the standard deviation of multiple models of TSI variability using different Mg and sunspot darkening indices and TSI observations. As an example, the modeled spectral irradiance uncertainties (excluding the uncertainty in the absolute spectral irradiance scale, $\sigma_{\text{quiet}(\lambda)}$), during Cycle 23 maximum at 200, 500, and 900 nm are of order 7%, 30%, and 20% of the energy increase during the cycle (Figure 6b).

3.4. Model Validation

Direct observations of solar spectral irradiance variability lack, as yet, the long-term repeatability needed to reliably track solar cycle changes (Lean & DeLand, 2012; Mauceri et al., 2018) and hence to validate spectral irradiance variability models on these time scales. One possible exception is the HI Lyman α irradiance at 121.56 nm for which the estimated repeatability of measurements by SOLSTICE on SORCE since 2003 is 5% compared with solar cycle changes of order 50% (Snow et al., 2018). Figure 7 shows that the NRLSSI3 model of spectral irradiance variability at 121.5 ± 0.5 nm reproduces the SOLSTICE observations in the same 1 nm bin slightly better than does the NRLSSI2 (CDR) model; the correlation of the model and observations increases marginally (from 0.987 to 0.988), the standard deviation of the model and observations decreases (from 0.121 to 0.113 mW m^{-2}) and the histogram of the residuals is more Gaussian-like (with FWHM decreasing from 0.282 to 0.241).

The newly constructed SIST composite of Lyman α irradiance observations at 121.5 nm provides a time series over a much longer duration (>40 years) than the 15 years of SOLSTICE observations (Machol et al., 2019). Analogous to Figure 7, Figure 8 compares with the SIST Lyman α composite irradiance since 1978 the variations at 121.5 nm according to the NRLSSI3 and NRLSSI2 (CDR) models. Contrary to the comparisons in Figure 7 of the models with the shorter duration but more precise SOLSTICE Lyman α irradiance, Figure 8 suggests that the NRLSSI3 model does not reproduce the SIST Lyman α irradiance variations better than the NRLSSI2 model. The correlation of the observations and model and the FWHM of the histogram of the residuals are essentially unchanged although the standard deviation of the residuals of the observations and model is slightly larger for NRLSSI3 than NRLSSI2 (0.233 vs 0.212 mW m^{-2}). The larger uncertainties in the composite record prior to the SORCE observations possibly limit its ability to properly validate the NRLSSI3 model.

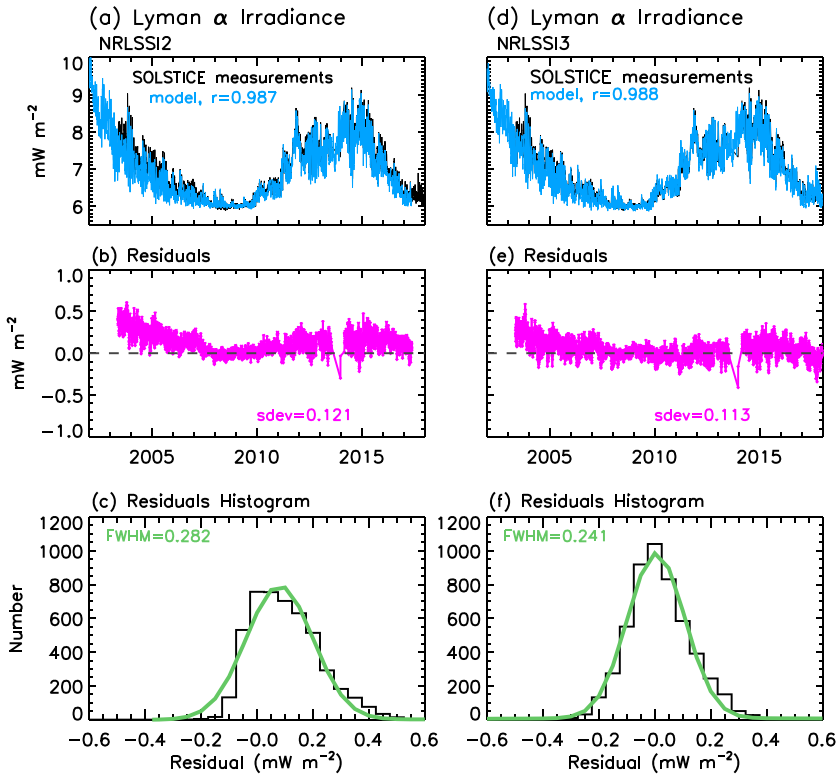

Figure 7. (a) The SORCE measurements of Lyman α spectral irradiance at 121.5 nm (black line) compared with the NRLSSI2 (NOAA CDR) model using the Bremen Mg index. (b) The residuals of the SORCE measurements and the NRLSSI2 model and (c) the histogram of the residuals. (d) Compared are the SORCE Lyman α irradiances and the NRLSSI3 model, also using the Bremen Mg index. (e) The residuals of the SORCE measurements and the NRLSSI3 model and (f) the histograms of the residuals. The green lines in (c) and (f) are Gaussian fits to the histograms of the residuals.

While quantitative comparisons of the NRLSSI3 model with direct spectral irradiance observations are problematic at wavelengths other than 121.5 nm, a partial validation of modeled irradiance variability at wavelengths between 265 and 500 nm is possible on shorter rotational time scales using the independent OMI database (Marchenko et al., 2019). Figure 9 compares time series of near-UV spectral irradiance at five different wavelengths in two different epochs (in 2012, on the left, and in 2014 on the right), detrended by removing 81-day running means to expose the variations (in energy units) on time scales of days to months. The NRLSSI3 model tracks the short-term spectral irradiance variability measured independently by OMI with high fidelity, matching the rotational modulation amplitude throughout the spectral range from 300 to 400 nm in both epochs. Also shown in Figure 9 is rotational modulation in the (similarly detrended) SATIRE model, which overestimates OMI rotational modulation at some, but not all, near-UV wavelengths (e.g., 315.5 and 375.5 nm), and in the (detrended) EMPIRE model, which systematical overestimates the magnitude of the short-term variations measured by OMI at essentially all near-UV wavelengths.

To better compare the spectral dependence of irradiance variability during solar rotation in the NRLSSI3, SATIRE, and EMPIRE models with the OMI observations, Figure 10 shows two independent, and quite different, metrics that numerically quantify the magnitude of these changes. Compared in Figure 10a are the average absolute deviations of the solar spectral irradiance at wavelengths from 265 to 500 nm, relative to 81-day running means. Compared in Figure 10b are the demodulated amplitudes (minimum to maximum) of the variability at a period of 27 days, calculated using complex demodulation (Bloomfield, 1976). Complex demodulation is a form of local harmonic analysis that captures the temporal evolution of the amplitude and phase of variability in a selected frequency band in a time series.

Both the standard deviations and the demodulated amplitudes of the magnitude of short-term (~27-day) spectral irradiance variations from 265 to 500 nm show the overall good agreement of the NRLSSI3 model and independent OMI observations; a notable exception is in the vicinity of the Fe I Fraunhofer line at

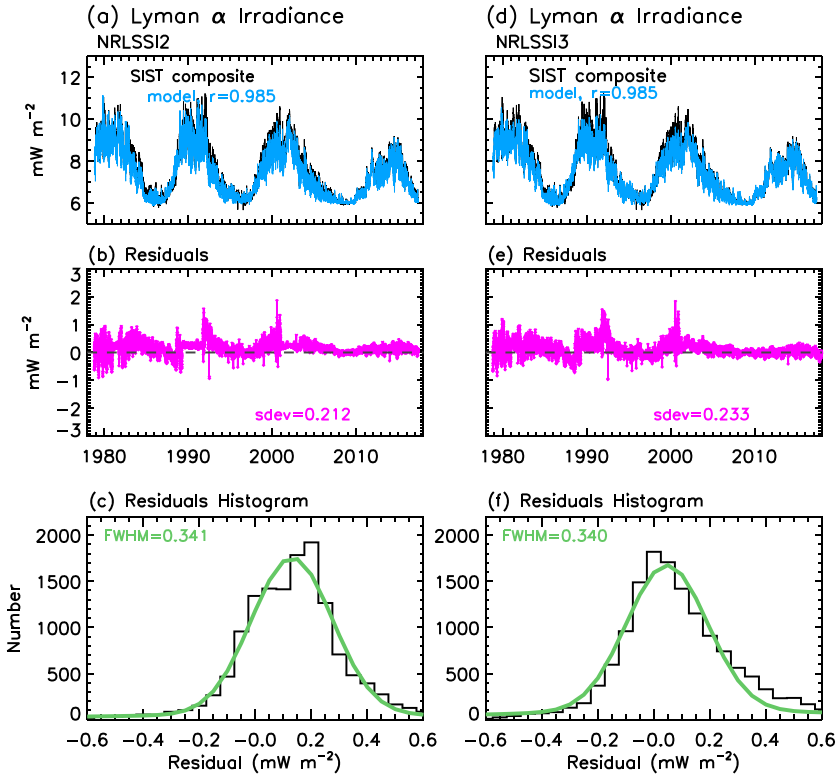

Figure 8. (a) The SIST composite record of observations of Lyman α spectral irradiance at 121.5 nm (black line) and the NRLSSI2 (NOAA CDR) model using the Bremen Mg index. (b) The residuals of the SIST observational composite and the NRLSSI2 model and (c) the histogram of the residuals. (d) Compared are the SIST Lyman α composite and the NRLSSI3 model, also using the Bremen Mg index. (e) The residuals of the SIST composite and the NRLSSI3 model and (f) the histogram of the residuals. The green lines in (c) and (f) are Gaussian fits to the histograms of the residuals.

382.04 whose variability the NRLSSI3 model overestimates relative to the OMI observations. Compared with the OMI observations, the SATIRE model overestimates short-term irradiance variability excessively in broad wavelength regions in the vicinity of most Fraunhofer lines (e.g., the Fe I lines at 382.0, 373.5, and 358.1 nm), while the EMPIRE model systematically overestimates the variability by 50% or more at essentially all wavelengths less than ~430 nm. At wavelengths from 430 to 500 nm, both the OMI observations and NRLSSI3 model show larger short-term spectral irradiance changes than both the SATIRE and EMPIRE models; the EMPIRE model, in particular, underestimates the rotational modulation of spectral irradiance variability in this region by more than a factor of two.

The direct TSI observations afford additional, albeit indirect, validation of modeled spectral irradiance variability. The assumption underlying this approach is that solar emissions emergent from similar regions of the solar atmosphere vary similarly. The equivalent effective temperature of formation of TSI is 5770 K which is comparable to the formation temperature of solar spectral emission near 650.5 nm (see Harder et al., 2009, Figure 2). Figure 11 thus compares the NRLSSI3 model of solar spectral irradiance variability at 650.5 nm with that of (scaled) TSI. As expected, the correlation is high (0.97); the standard deviation of the residuals of the NRLSSI3 650.5 nm time series with the (scaled) TIM TSI variations, shown in Figure 11b is 0.00012 W m^{-2}, which is 0.008% of the absolute irradiance and 12% of the irradiance increase of ~0.001 W m^{-2} during the solar cycle. Neither the SATIRE nor EMPIRE models of SSI variability at 650.5 nm track the (scaled) TIM TSI variations as well as does the NRLSSI3 model; the standard deviations of the residuals of the SATIRE model is 0.00021 (0.013%, Figure 11c) and of the EMPIRE model is 0.00017 (0.011%, Figure 11d). Figure 11e further shows that the correlation with TIM TSI observations of the NRLSSI3 model is higher at all wavelengths from 600 to 1,000 nm than are the correlations of either the SATIRE or EMPIRE models.

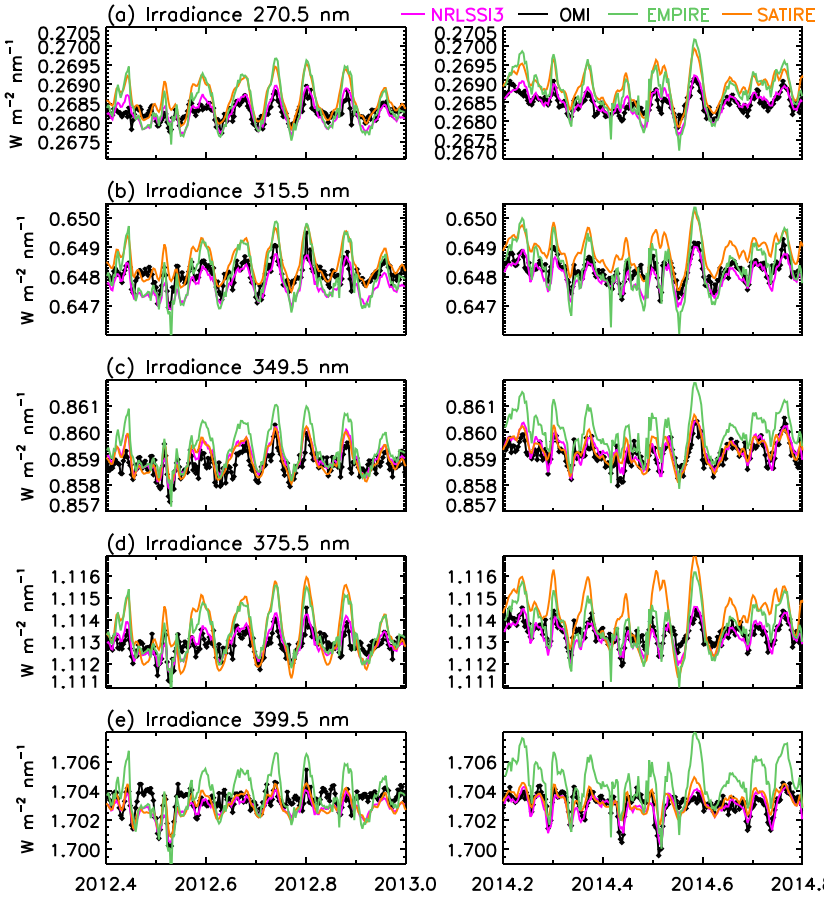

Figure 9. Compared for two different epochs, in 2012 on the left and 2014 on the right, are solar spectral irradiance variations in the middle ultraviolet spectrum observed by OMI (black) and estimated by the NRLSSI3 (magenta), SATIRE (orange), and EMPIRE (green) models at (a) 270.5 nm, (b) 315.5 nm, (c) 349.5 nm, (d) 375.5 nm, and (e) 399.5 nm. Longer-term trends have been removed from the measurement and model time series.

While not conclusive, the comparisons in Figure 11 of modeled spectral irradiance variations with the (scaled) concurrent TIM TSI variations suggest that the NRLSSI3 model better captures the time dependence of solar variability at most visible and near-infrared wavelengths than do either the SATIRE or EMPIRE models. The SATIRE spectral irradiance variations have a systematic solar cycle drift relative to the TIM TSI observations that contributes to the higher standard deviation of the SATIRE spectral irradiance model residuals, such as Figure 11c illustrates at 650.5 nm. In contrast, larger short-term fluctuations contribute to the larger standard deviation of the residuals of the EMPIRE model and (scaled) TIM TSI observations, possibly because of EMPIRE's use of the Balmaceda et al. (2009) sunspot darkening index, which section 2.3 established as inferior relative to the Debrecen and SOON sunspot indices in reproducing TSI variability.

4. Discussion

4.1. Total Solar Irradiance Variability

It is well established that faculae and sunspots are the primary sources of solar irradiance variability and that model parameterizations of these magnetic features readily reproduce the observations. As the fidelity of a model's facular and sunspot representations improves, so too does its ability to reproduce observed irradiance variability. Using a facular component constructed with a linear and nonlinear Mg index and sunspot component constructed using observations of sunspot areas and locations in the Debrecen catalog, the NRLTSI3 model captures a higher fraction of TSI variance in 39+ years of independent observations than do extant models of TSI variability. It explains, on average, 80% of the variance in daily values in six

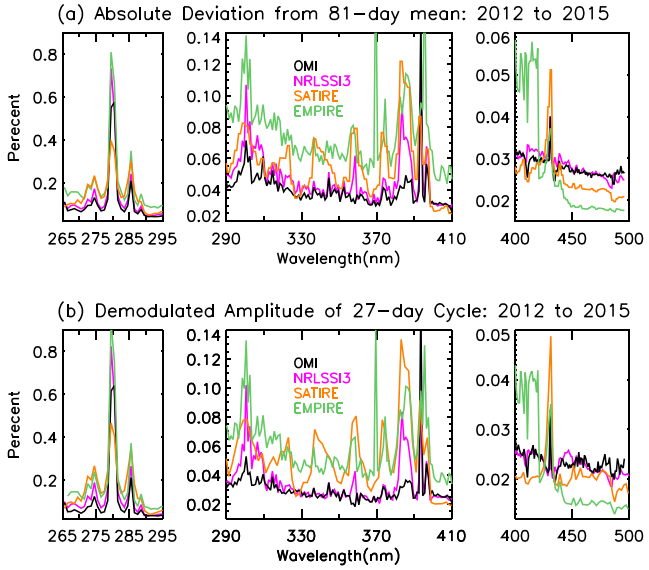

Figure 10. Compared are the magnitudes of rotational modulation of solar spectral irradiance at wavelengths between 265 and 500 nm in the OMI observations (black) and the NRLSSI3 (magenta), SATIRE (orange), and EMPIRE (green) models, estimated in two different ways, using (a) the standard deviation of the time series relative to 81-day means and (b) the magnitude of the 27-day cycle, extracted using complex demodulation.

independent TSI observational composite records from 1978 to 2017 (average correlation of 0.892); the NRLTSI2 and SATIRE models explain, on average, 79% and 72% of the observed variance in the same six observational composites (average correlation coefficients of 0.888 and 0.849, respectively, Table 3).

The traditional technique of constructing a composite record by cross calibrating overlapping databases, which PMOD uses, may be as good as the approach of statistically isolating and recombining variance at selected periods used to construct the SOLID and SIST composites. The PMOD composite agrees better with all three NRLTSI3, NRLTSI2, and SATIRE models than do any of the five other composites. The highest correlation among the six observational composites and three models of TSI variability is between the PMOD composite and the NRLTSI3 model (correlation coefficient 0.939); for comparison, the correlations of the SOLID-C and SIST TSI composites with NRLTSI3 are 0.915 and 0.906, respectively (Table 3). The lowest correlation among the six observational composites and three models of TSI variability is between the SOLID composite and the SATIRE model (correlation coefficient 0.796).

Different long-term trends in the TSI composite records and models of TSI variability are a primary reason for differences among the observations and models. For 12,863 common daily values in the PMOD, SOLID-C and SIST TSI composites and the NRLTSI3, NRLTSI2, and SATIRE models from 1978 to 2017, the trends of -5.6 ± 2 ppm per year in the PMOD composite, -6 ± 2 ppm per year in the NRLTSI3 model and -4 ± 2 ppm per year in the NRLTSI2-CDR model agree to within their mutual 1σ uncertainties (taking into account autocorrelation). In contrast, the trends of -1 ± 2 and $\sim 0 \pm 2$ ppm per year in the SOLID-C and SIST composites are less negative than in the PMOD composite and the NRLTSI3 and NRLTSI2 models. There is a prominent linear trend of -13 ± 2 ppm per year in the SATIRE model that exceeds the trends in both the NRLTSI3 and NRLTSI2 models and in the PMOD, SOLID-C, and SIST observational composites, with the differences exceeding their mutual uncertainties in all cases. This trend is a likely reason why SATIRE does not reproduce the multidecadal TSI composites as well as does the NRLTSI3 or NRLTSI2 models.

The linear trend in the SATIRE model of TSI variability over more than three solar cycles is likely spurious since it is a factor of two or more larger than trends in both the NRLTSI3 model and the observational composites. To better assess multidecadal trends and solar cycle amplitudes, Figure 12a compares annual values of the NRLTSI3 and SATIRE models with observational composite records of TSI over the past ~40 years. Especially prominent is the deviation of the SATIRE model from the NRLTSI3 model and observations prior to 1996. Figure 12a shows that SATIRE's TSI value in the 1986 cycle minimum is ~0.4 W m^{-2} higher than in the 2009 cycle minimum whereas in the TSI composites and the NRLTSI3 model TSI levels are comparable or lower in 1986 than in 2009. SATIRE's overestimation of the 1986 cycle minimum level results in its distinct underestimation of the magnitude of Solar Cycle 21 relative to the observational composites and the NRLTSI3 model. The origin of SATIRE's spurious Cycle 21 amplitude and inter minima trend may be its use of ground-based solar magnetograms to estimate its two facular components, prior to availability of the space-based SOHO magnetograms in 1996. Faculae are more dispersed over the solar disc and have lower contrast than sunspots, making it difficult to determine their disc-integrated signal with adequate long-term stability using an index derived from spatially resolved, rather than irradiance, observations. This is especially true when using measurements made by ground-based magnetograms which themselves have uncertain calibration and repeatability.

4.2. Solar Spectral Irradiance Variability

Solar irradiance varies differently throughout the spectrum because the contrasts of the faculae and sunspots that alter the background emission depend on wavelength. The new NRLSSI3 model determines the relative contributions of these two features by multiple regression of spectral irradiance observations against facular

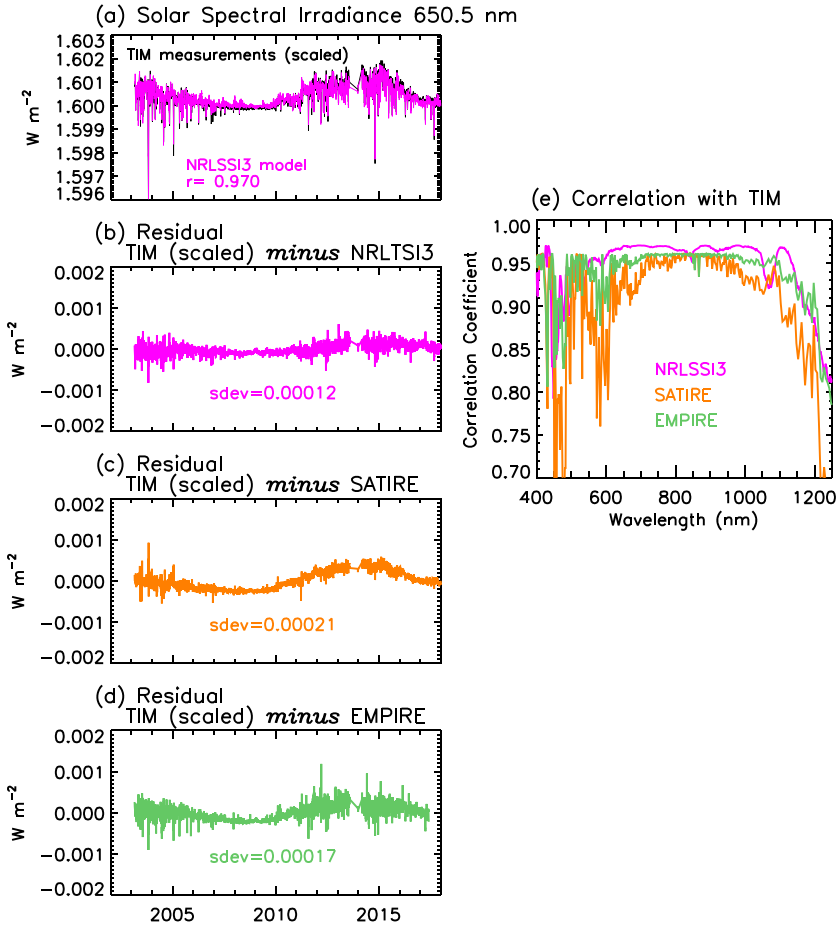

Figure 11. (a) Compared with the (scaled) TIM measurements of total solar irradiance are the NRLSSI3 model estimates of solar spectral irradiance at 650.5 nm (magenta), whose formation temperature of 5770 K is similar to the equivalent effective temperature of formation of TSI. The residuals of the observed (scaled) TSI observations and modeled spectral irradiance variations at 650.5 nm are shown (b) for NRLSSI3, (c) SATIRE, and (d) EMPIRE. (e) The correlations of the TIM TSI observations with the spectral irradiance at wavelengths from 400 to 1,250 nm estimated by the NRLSSI3 (magenta), SATIRE (orange), and EMPIRE (green) models.

and sunspot indices. The SATIRE model achieves this using contrast factors estimated by theoretical stellar atmosphere models (Unruh et al., 2000).

The good agreement between the NRLSSI3 model and the independent OMI observations (not used to construct the model) of the rotational modulation of solar spectral irradiance suggests that the spectral dependence of NRLSSI3's facular and sunspot components are robust, at least for wavelengths less than 500 nm. At wavelengths corresponding to the Sun's near-UV continuum emission the magnitude of spectral irradiance rotational modulation in the SATIRE model also agrees well with the OMI observations and the NRLSSI3 model. The SATIRE model, however, significantly overestimates rotational modulation of spectral irradiance in the vicinity of Fraunhofer lines. Prior work also suggests that the SATIRE model overestimates the variability of spectral features at UV wavelengths (Unruh et al., 2008) because of limitations of the theoretical stellar atmosphere model used to estimate the facular and sunspot contrasts. These limitations include the assumption of local thermodynamical equilibrium and the difficulty in specifying "line blanketing," the extensive absorption of the photospheric radiation continuum by species in the Sun's overlying solar atmosphere (Shapiro et al., 2015).

Shown in Figure 13 are estimates of the facular and sunspot contrasts derived from the coefficients of the NRLSSI3 model (by normalizing to the quiet spectrum). These observation-derived values are scaled to match the absolute values of the SATIRE model's facular and sunspot contrasts at visible and

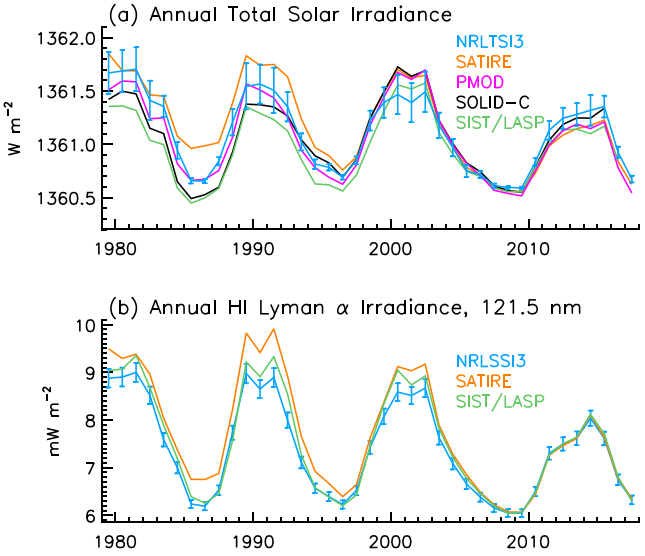

Figure 12. (a) Compared are annual values of the NRLTSI3 model of total solar irradiance (blue), with uncertainties, and the SATIRE model (orange) with three different observational composite records of TSI: PMOD (magenta), SOLID-C (black), and SIST (green). (b) Compared are annual values of the NRLSSI3 model of solar Lyman α spectral irradiance (blue), with uncertainties, and the SATIRE model (orange) with the SIST observational composite record (green).

near-infrared wavelengths, determined by a theoretical stellar atmosphere model (Unruh, private communication, April 2018). The comparisons suggest that in addition to overestimating the brightness of faculae in the vicinity of major Fraunhofer lines (indicated by dashed vertical lines in Figure 13a) in the middle UV spectral region, SATIRE's stellar atmosphere model may also underestimate the sunspot darkening in both this region, and possibly in the near-infrared spectrum.

Differences between the observationally derived and theoretically specified facular and sunspot contrasts in Figure 13 are a primary cause of differences in the magnitude of spectral irradiance variability estimated by the NRLSSI3 and SATIRE models during the solar cycle as well as during solar rotation. For example, from solar activity minimum (2009.0–2009.2, Figure 6) to Cycle 24 maximum (2013.5–2013.8, Figure 6), solar irradiance in the wavelength band from 300 to 400 nm increases 0.206 W m^{-2} in NRLSS3 model and 0.226 W m^{-2} in the SATIRE model. At the same time, visible irradiance from 500 to 750 nm increases 0.258 W m^{-2} in the NRLSSI3 model and 0.157 W m^{-2} in the SATIRE model.

It is argued, incorrectly, that the larger variability in the EMPIRE model in the region 300–400 nm validates the SATIRE model (Yeo et al., 2017). In reality, spectral irradiance variability in the EMPIRE and SATIRE models differ notably in a number of ways. First, the increase from Solar Cycle 24 minimum to maximum of 0.280 W m^{-2} at 300 to 400 nm in the EMPIRE model exceeds the increase of 0.226 W m^{-2} in the SATIRE model (this latter model agrees better with the NRLSSI3 model's increase of 0.206 W m^{-2}). Second, the EMPIRE model systematically overestimates rotational modulation throughout the entire middle UV spectrum, not just in Fraunhofer lines (as the SATIRE model does). This suggests that, independently of wavelength, EMPIRE's model coefficients overestimate the irradiance changes per given change in predictors at wavelengths less than ~420 nm. This may be because of the use of orthogonal distance regression to estimate the model coefficients. It is well recognized that misapplication of orthogonal distance regression can produce spurious results (e.g., Carroll & Ruppert, 1996; Coddington et al., 2019), as a result, for example, of poor model formulation and/or lack of reliable knowledge of the predictor uncertainties, a priori estimates of which orthogonal distance regression requires.

The requirement that integrated spectral irradiance variability matches that of TSI necessitates that a consequence of EMPIRE's systematic overestimation of spectral irradiance variability and SATIRE's overestimation of spectral irradiance variability in Fraunhofer lines at wavelengths less than 420 nm, is the simultaneous underestimation by these models (in different amounts) of spectral irradiance variability at longer wavelengths; the increase during Solar Cycle 24, for example, at 500–750 nm is 0.191 W m^{-2} in the EMPIRE model and 0.157 W m^{-2} in the SATIRE model, compared with 0.258 W m^{-2} in the NRLSSI3 model.

Differences in long-term trends in solar spectral irradiance over the past 40 years in the NRLSSI3 and SATIRE models mimic the differences in the long-term trends in total solar irradiance in the corresponding NRLTSI3 and SATIRE models. Figure 12b shows that whereas in both the NRLSSI3 model and the SIST observational composite, the solar Lyman α emission in 1986 is ~0.2 mW m^{-2} higher than in 2009, in the SATIRE model it is ~0.7 mW m^{-2}. This suggests that SATIRE's declining Lyman α irradiance from 1986 to 2009, like its declining trend in TSI over this same period, is spurious, and likely traceable to the same cause, namely the lack of long-term repeatability in the SATIRE's facular indices derived from ground-based magnetograms. However the Lyman α spectral irradiance database may lack sufficient long-term stability to quantify long-term spectral irradiance trends.

5. Summary

New models of solar total and spectral irradiance variability derived from SORCE observations since 2003 and utilizing improved facular and sunspot inputs reproduce observed irradiance variations with higher

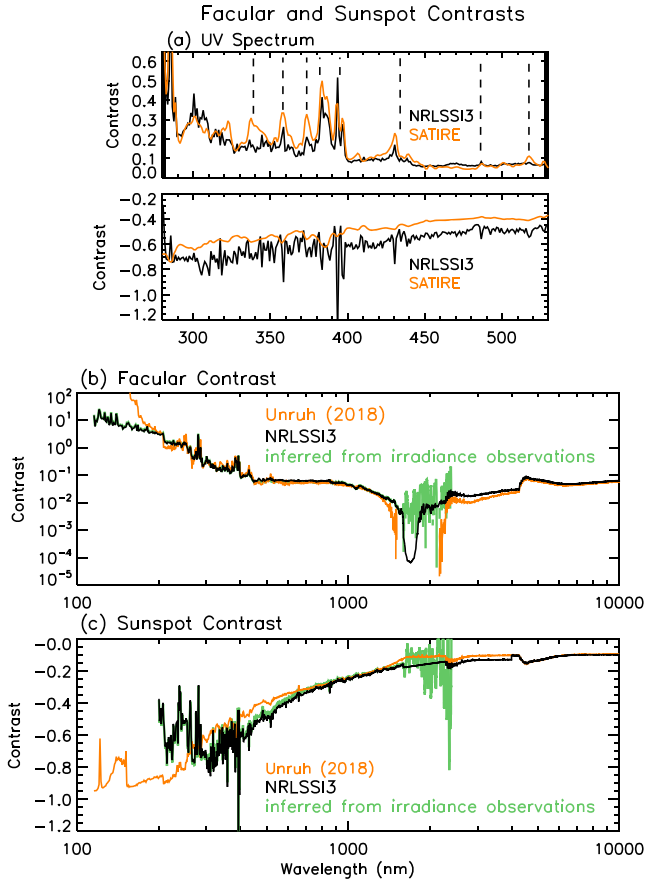

Figure 13. Compared are the contrasts of faculae and sunspots pertaining to the NRLSSI3 (black) and SATIRE (orange) models. The contrasts for NRLSSI3 are determined by dividing the model's facular and sunspots coefficients by the quiet spectral irradiance then scaling to the magnitude of the SATIRE model's contrasts in the visible and near-infrared wavelength region. (a) The contrasts for wavelengths from 280 to 530 nm. The dashed vertical lines indicate the locations of some prominent Fraunhofer lines in the solar spectrum. (b and c) The contrasts are compared across a broader wavelength range from 100 to 10,000 nm. The contrasts derived from the coefficients of the NRLSSI3 model (black) are scaled to match those used in SATIRE (orange) estimated by theoretical stellar atmosphere models in the visible spectral region. The green lines in (b) and (c) are the coefficients derived directly from the SORCE observations. Because of their large scatter at wavelengths from 1,600 to 2,300 nm, the model adopts the smooth black line to estimate spectral irradiance variability.

fidelity than extant models, according to comparisons with independent total and spectral irradiance observations.

The new NRLTSI3 model of total solar irradiance variability accounts for 67% to 88% percent of the variance in six independent, differently constructed observational composite records and its trend over the period from 1984 to 2013 (for which all six composite records exist) of -4 ± 3 ppm per year agrees with trends in the observational composites, which range from -4 ± 3 ppm per year in the PMOD composite to 3 ± 3 in the SIST composite, to within their mutual uncertainties. In comparison over this same time period the SATIRE model explains a smaller fraction of the variance in the observational composites (65% to 83%) and its trend of -14 ± 3 ppm per year exceeds that in all six composites (and in the NRLTSI3 model) by more than a factor of 3.

The new NRLSSI3 model of spectral irradiance variability closely tracks the rotational modulation of the independent OMI observations at all available wavelengths from 265 to 500 nm, suggesting that the model's parameterizations of the relative facular and sunspot influences are robust. Both the SATIRE and EMPIRE models overestimate the OMI rotational modulation suggesting that their facular and sunspot parameterizations are less well specified. In the case of the SATIRE model, the significant overestimation of middle UV Fraunhofer lines may be a consequence of that model's use of facular and sunspot contrasts estimated using theoretical stellar astrophysical models that assume thermodynamical equilibrium in the formation of the lines and the difficulty in properly quantifying line blanketing by the Sun's atmosphere of the underlying continuum emission. In the case of the EMPIRE model the systematic overestimation of middle UV rotational modulation by a factor of ~50% is likely linked to the limitations of orthogonal distance regression to properly constrain that model's coefficients.

Except for the Lyman α emission at 121.5 nm, it is not possible to validate the magnitude of spectral irradiance variations at most wavelengths during the solar cycle in the new NRLSSI3 model, because of the lack of repeatability of the observational database. The NRLSSI3 model tracks the new SIST Lyman α observational composites to within their combined uncertainties but the SATIRE model's Lyman α spectral irradiance, like its TSI, has a larger multidecadal trend than both the observational composite and the NRLSSI3 model. The disagreement of the SATIRE model's long-term irradiance trends as well as its underestimation of the magnitude of irradiance variability in Solar Cycle 21 suggests that its long-term trend is spurious. A possible cause is the use of facular inputs derived from ground-based solar magnetograms prior to the availability of space-based observations in 1996; it is difficult, if not impossible, to secure the needed long-term stability from ground-based spatially resolved observations with unmonitored calibration drifts.

It is expected that the new NRLTSI3 and NRLSSI3 models will contribute to a new version of the NOAA Solar Irradiance CDR, following extension of the models prior to 1978 and further improvements and validation using independent observations. New irradiance observations commenced in 2017 with the launch of the Total Solar irradiance Monitor (TSIS) on the Space Station (Richard et al., 2011) and new spectral irradiance composite records have been developed as part of the SIST (DeLand, Kopp, & Considine, 2019). Preliminary estimates suggest that the repeatabilities of the TSIS total and spectral irradiance measurements exceed those of prior measurements. These superior observations will enable improved validation of both the existing CDR and new models, using the multiple metrics developed in this paper to assess the performance of the models with existing observations. A particular focus of future work is improved

characterization of irradiance variability in the spectral region longward of 900 nm, where the new TSIS observations have substantially higher repeatability than the extant SORCE measurements used to construct the NRLSSI3 model.

Data Availability Statement

SORCE data are available at http://lasp.colorado.edu/home/sorce/. The Bremen Mg index is at http://www.iup.uni-bremen.de/UVSAT/Datasets/mgii. Sunspot region information is at http://www.ngdc.noaa.gov/stp/spaceweather.html. Table 1 lists additional data sources produced by many scientists, whose efforts we gratefully acknowledge. Provided as Supplemental Material are files of daily NRLTSI3 total solar irradiance and Lyman α irradiance, including uncertainties, a file of daily NRLSSI3 solar spectral irradiance in 3785 wavelengths bins, and a separate file of uncertainties, from 1978 to 2017.

Acknowledgments

NASA supported the construction of the NRLTSI3 and NRLSSI3 models as part of the SIST program. NOAA funded the development and transition of the Solar Irradiance Climate Data Record. We thank Yvonne Unruh for providing the theoretical facular and sunspot contrasts. We acknowledge and appreciate collaboration with our late colleague Tunde Baranyi and her sustained effort in producing the Debrecen sunspot catalog.

References

Balmaceda, L. A., Solanki, S. K., Krivova, N. A., & Foster, S. (2009). A homogeneous database of sunspot areas covering more than 130 years. *Journal of Geophysical Research*, *114*, A07104. https://doi.org/10.1029/2009JA014299

Bloomfield, P. (1976). *Fourier analysis of time series: An introduction*. New York: John Wiley and Sons.

Carroll, R. J., & Ruppert, D. (1996). The use and misuse of orthogonal regression in linear errors-in-variables models. *The American Statistician*, *50*(1), 1–6.

Chai, T., & Draxler, R. R. (2014). Root mean square error (RMSE) or mean absolute error (MAE)?—Arguments against avoiding RMSE in the literature. *Geoscientific Model Development*, *7*(3), 1247–1250. https://doi.org/10.5194/gmd-7-1247-2014

Coddington, O., & Lean, J. (2015). Climate algorithm theoretical basis document: Total solar irradiance and solar spectral irradiance. NOAA CRDP-ATBD-0612, 56 pp.

Coddington, O., Lean, J., Pilewskie, P., Snow, M., Richard, E., Kopp, G., et al. (2019). Solar irradiance variability: Comparisons of models and measurements. *Earth and Space Science*, *6*, 2525–2555. https://doi.org/10.1029/2019EA000693

Coddington, O., Lean, J. L., Pilewskie, P., Snow, M., & Lindholm, D. (2016). A solar irradiance climate data record. *BAMS*, *97*(7), 1265–1282. https://doi.org/10.1175/BAMS-D-14-00265.1

DeLand, M. T., & Cebula, R. P. (1993). Composite Mg II solar activity index for solar Cycles 21 and 22. *Journal of Geophysical Research*, *98*(D7), 12,809–12,823. https://doi.org/10.1029/93JD00421

DeLand, M. T., & Cebula, R. P. (1998). NOAA 11 Solar Backscatter Ultraviolet, model 2 (SBUV/2) instrument solar spectral irradiance measurements in 1989–1994: 2. Results, validation, and comparisons. *Journal of Geophysical Research*, *103*(D13), 16,251–16,273. https://doi.org/10.1029/98JD01204

DeLand, M. T., & Cebula, R. P. (2008). Creation of a composite solar ultraviolet irradiance data set. *Journal of Geophysical Research*, *113*, A11103. https://doi.org/10.1029/2008JA013401

DeLand, M. T., & Cebula, R. P. (2012). Solar UV variations during the decline of Cycle 23. *Journal of Atmospheric and Solar-Terrestrial Physics*, *77*, 225–234. https://doi.org/10.1016/j.jastp.2012.01.007

DeLand, M. T., Floyd, L. E., Marchenko, S., & Tiruchirapalli, R. (2019). Creation of the GSFCSSI2 composite solar spectral irradiance data set. *Earth and Space Science*, *6*, 1284–1298. https://doi.org/10.1029/2019EA000616

DeLand, M. T., Kopp, G., & Considine, D. B. (2019). Overview of the NASA Solar Irradiance Science Team (SIST) program special section. *Earth and Space Science*, *6*, 2229–2231. https://doi.org/10.1029/2019EA000773

Dewitte, S., & Nevens, S. (2016). The total solar irradiance climate data record. *The Astrophysical Journal*, *830*(1), 25. https://doi.org/10.3847/0004-637X/830/1/25

Dudok de Wit, T., Kopp, G., Fröhlich, C., & Schöll, M. (2017). Methodology to create a new total solar irradiance record: Making a composite out of multiple data records. *Geophysical Research Letters*, *44*, 1196–1203. https://doi.org/10.1002/2016GL071866

Ermolli, I., Matthes, K., Dudok de Wit, T., Krivova, N. A., Tourpali, K., Weber, M., et al. (2013). Recent variability of the solar spectral irradiance and its impact on climate modelling. *Atmospheric Chemistry and Physics*, *13*(8), 3945–3977. https://doi.org/10.5194/acp-13-3945-2013

Foukal, P. (1981). Sunspots and changes in the global output of the Sun. In L. Cram, & J. Thomas (Eds.), *The physics of sunspots* (pp. 391–423). Sunspot NM: Sacramento Peak Observatory.

Fröhlich, C. (2006). Solar irradiance variability since 1978. *Space Science Reviews*, *125*(1-4), 53–65. https://doi.org/10.1007/s11214-006-9046-5

Fröhlich, C. (2013). Total solar irradiance: What have we learned from the last three cycles and the recent minimum? *Space Science Reviews*, *176*(1-4), 237–252. https://doi.org/10.1007/s11214-011-9780-1

Fröhlich, C., & Lean, J. (2004). Solar radiative output and its variability: Evidence and mechanisms. *Astronomy and Astrophysics Review*, *12*(4), 273–320. https://doi.org/10.1007/s00159-004-0024-1

Gray, L. J., Beer, J., Geller, M., Haigh, J. D., Lockwood, M., Matthes, K., et al. (2010). Solar influences on climate. *Reviews of Geophysics*, *48*, RG4001. https://doi.org/10.1029/2009RG000282

Győri, L., Baranyi, T., & Ludmány, A. (2011). Photospheric data programs at the Debrecen Observatory. Proc. Of the Intern. Astron. Union, 6, Symp. S273, https://doi.org/10.1017/S174392131101564X

Haberreiter, M., Schöll, M., Dudok de Wit, T., Kretzschmar, M., Misios, S., Tourpali, K., & Schmutz, W. (2017). A new observational solar irradiance composite. *Journal of Geophysical Research: Space Physics*, *122*, 5910–5930. https://doi.org/10.1002/2016JA023492

Harder, J., Thuillier, G., Richard, E. C., Brown, S. W., Lykke, K. R., Snow, M., et al. (2010). The SORCE SIM solar spectrum: Comparison with recent observations. *Solar Physics*, *263*(1-2), 3–24. https://doi.org/10.1007/s11207-010-9555-y

Harder, J. W., Fontenla, J. M., Pilewskie, P., Richard, E. C., & Woods, T. N. (2009). Trends in solar spectral irradiance variability in the visible and infrared. *Geophysical Research Letters*, *36*, L07801. https://doi.org/10.1029/2008GL036797

Jungclaus, J. H., Bard, E., Baroni, M., Braconnot, P., Cao, J., Chini, L. P., et al. (2017). The PMIP4 contribution to CMIP6—Part 3: The last millennium, scientific objective and experimental design for the PMIP4 past 1000 simulations. *Geoscientific Model Development*, *10*(11), 4005–4033. https://doi.org/10.5194/gmd-2016-278

Kopp, G. (2014). An assessment of the solar irradiance record for climate studies. *Space Weather Space Climate*, *4*, A14. https://doi.org/10.1051/swsc/2014012

Kopp, G., Heuerman, K., Harber, D., & Drake, V. (2007). The TSI radiometer facility—Absolute calibrations for total solar irradiance instruments. *SPIE*, *6677*, 667,709. https://doi.org/10.1117/12.734553

Kopp, G., Lawrence, G., & Rottman, G. (2005). The Total Irradiance Monitor (TIM): Science results. *Solar Physics*, *230*(1-2), 129–139. https://doi.org/10.1007/s11207-005-7433-9

Kopp, G., & Lean, J. (2011). A new, lower value of total solar irradiance: Evidence and climate significance. *Geophysical Research Letters*, *38*, L01706. https://doi.org/10.1029/2010GL045777

Krivova, N. A., Solanki, S. K., & Unruh, Y. C. (2011). Towards a long-term record of solar total and spectral irradiance. *Journal of Atmospheric and Solar-Terrestrial Physics*, *73*(2-3), 223–234. https://doi.org/10.1016/j.jastp.2009.11.013

Krivova, N. A., Vieira, L. E. A., & Solanki, S. K. (2010). Reconstruction of solar spectral irradiance since the Maunder minimum. *Journal of Geophysical Research*, *115*, A12112. https://doi.org/10.1029/2010JA015431

Kurucz, R. L. (1991). *The solar spectrum*. In A. N. Cox, W. C. Livingston, & M. S. Matthews (Eds.), Solar interior and atmosphere. Tucson: the University of Arizona Press.

Lean, J., Rottman, G., Harder, J., & Kopp, G. (2005). SORCE contributions to new understanding of global change and solar variability. *Solar Physics*, *230*(1-2), 27–53. https://doi.org/10.1007/s11207-005-1527-2

Lean, J. L. (2017). *Sun-climate connections*, Oxford: Oxford Research Encyclopedia of Climate. https://oxfordre.com/climatescience/view/10.1093/acrefore/9780190228620.001.0001/acrefore-9780190228620-e-9

Lean, J. L., Cook, J., Marquette, W., & Johannesson, A. (1998). Magnetic sources of the solar irradiance cycle. *The Astrophysical Journal*, *492*(1), 390–401. https://doi.org/10.1086/305015

Lean, J. L., & DeLand, M. T. (2012). How does the Sun's spectrum vary? *Journal of Climate*, *25*, 2555–2560. https://doi.org/10.1175/JCLI-D-11-00571.1

Machol, J., Snow, M., Woodraska, D., Woods, T., Viereck, R., & Coddington, O. (2019). An improved Lyman-alpha composite. *Earth and Space Science*, 2263–2272. https://doi.org/10.1029/2019EA000648

Marchenko, S. V., & DeLand, M. T. (2014). Solar spectral irradiance changes during Cycle 24. *The Astrophysical Journal*, *789*(2), 117. https://doi.org/10.1088/0004-637X/789/2/117

Marchenko, S. V., DeLand, M. T., & Lean, J. L. (2016). Solar spectral irradiance variability in Cycle 24: Observations and models. *Journal of Space Weather and Space Climate*, *6*, A40. https://doi.org/10.1051/swsc/2016036

Marchenko, S. V., Woods, T. N., DeLand, M. T., Mauceri, S., Pilewskie, P., & Haberreiter, M. (2019). Improved Aura/OMI solar spectral irradiance: Comparisons with independent datasets and model predictions. *Earth and Space Science*, *6*, 2379–2396. https://doi.org/10.1029/2019EA000624

Matthes, K., Funke, B., Andersson, M., Barnard, L., Beer, J., et al. (2017). Solar forcing for CMIP6 (v3.2). *Geoscientific Model Development*, Katlenburg-Lindau, *10*, 2247–2302.

Mauceri, S., Pilewskie, P., Richard, E., Coddington, O., Harder, J., & Woods, T. (2018). Revision of the Sun's spectral irradiance as measured by SORCE SIM. *Solar Physics*, *293*, 161. https://doi.org/10.1007/s11207-018-1379-1

NASEM, National Academies of Science, Engineering and Medicine (2015). *Continuity of NASA Earth observations from space: A value framework*. Washington, DC: National Academies Press.

Richard, E., Harber, D., Rutkowski, J., O'Malia, K., Triplett, M., Drake, G., et al. (2011), Future long-term measurements of solar spectral irradiance by the TSIS spectral irradiance monitor: Improvements in measurement accuracy and stability, *Proceedings 11th International Conference on New Developments and Applications in Optical Radiometry*, Maui, HI, S. Park and E. Ikonen, Eds., paper INV004.

Roscoe, H. K., & Haigh, J. D. (2007). Influences of ozone depletion, the solar cycle and the QBO on the southern annular mode. *Quarterly Journal of the Royal Meteorological Society*, *133*(628), 1855–1864. https://doi.org/10.1002/qj.153

Rottman, G. (2005). The SORCE mission. *Solar Physics*, *230*(1-2), 7–25. https://doi.org/10.1007/s11207-005-8112-6

Rottman, G. (2006). Measurements of total and spectral solar irradiance. *Space Science Reviews*, *125*(1-4), 39–51. https://doi.org/10.1007/s11214-006-9045-6

Rottman, G., Harder, J., & Fontenla, J. (2005). The Spectral Irradiance Monitor (SIM): Early observations. *Solar Physics*, *230*(1-2), 205–224. https://doi.org/10.1007/s11207-005-1530-7

Scafetta, N., & Willson, R. C. (2014). ACRIM total solar irradiance satellite composite validation versus TSI proxy models. *Astrophysics and Space Science*, *350*(2), 421–442. https://doi.org/10.1007/s10509-013-1775-9

Shapiro, A. I., Solanki, S. K., Krivova, N. A., Tagirov, R. V., & Schmutz, W. K. (2015). The role of the Fraunhofer lines in solar brightness variability. *Astronomy and Astrophysics*, *581*, A116. https://doi.org/10.1051/0004-6361/201526483

Skupin, J., Weber, M., Bovensmann, H., & Burrows, J. P. (2004), The Mg II solar activity proxy indicator derived from GOME and SCIAMACHY, Proceedings of the ENVISAT & ERS Symposium (SP-572), ESA Publications Division.

Snow, M., Eparvier, F., Harder, J., Jones, A., McClintock, W., Richard, E., & Woods, T. (2018). Ultraviolet solar spectral irradiance variation on solar cycle timescales. *Proceedings of the International Astronomical Union*, *13*(S340), 203–208. https://doi.org/10.1017/S1743921318001278

Snow, M., McClintock, W. E., & Woods, T. N. (2010). Solar spectral irradiance variability in the ultraviolet from SORCE and UARS SOLSTICE. *Advances in Space Research*, *46*(3), 296–302. https://doi.org/10.1016/j.asr.2010.03.027

Snow, M., McClintock, W. E., Woods, T. N., White, O. R., Harder, J. W., & Rottman, G. (2005). The Mg II index from SORCE. In G. Rottman, T. Woods, & V. George (Eds.), *The Solar Radiation and Climate Experiment (SORCE)*. (Vol. 230, pp. 325–344). New York, NY: Springer. https://doi.org/10.1007/s11207-005-6879-0

Snow, M. J., Weber, M., Machol, J., Viereck, R., & Richard, E. (2014). Comparison of magnesium II core-to-wing ratio observations during solar minimum 23/24. *Space Weather Space Climate*, *4*, A04. https://doi.org/10.1051/swsc/2014001

Thuillier, G., DeLand, M., Shapiro, A., Schmutz, W., Bolsée, D., & Melo, S. M. L. (2012). The solar spectral irradiance as a function of the Mg II index for atmosphere and climate modelling. *Solar Physics*, *277*(2), 245–266. https://doi.org/10.1007/s11207-011-9912-5

Thuillier, G., Hersé, M., Simon, P. C., Labs, D., Mandel, H., Gillotay, D., & Foujols, T. (1998). The visible solar spectral irradiance from 350 to 850 nm as measured by the SOLSPEC spectrometer during the ATLAS I mission. *Solar Physics*, *177*(1/2), 41–61. https://doi.org/10.1023/A:1004953215589

Unruh, Y. C., Krivova, N. A., Solanki, S. K., Harder, J. W., & Kopp, G. (2008). Spectral irradiance variations: Comparison between observations and the SATIRE model on solar rotation time scales. *A&A*, *486*(1), 311–323. https://doi.org/10.1051/0004-6361:20078421

Unruh, Y. C., Solanki, S. K., & Fligge, M. (2000). Modelling solar irradiance variations: Comparison with observations, including line-ratio variations. *Space Science Reviews*, *94*(1/2), 145–152. https://doi.org/10.1023/A:1026758904332

Viereck, R., Puga, L., McMullin, D., Judge, D., Weber, M., & Tobiska, W. K. (2001). A proxy for solar EUV. *Geophysical Research Letters*, *28*(7), 1343–1346. https://doi.org/10.1029/2000GL012551

Viereck, R. A., Floyd, L. E., Crane, P. C., Woods, T. N., Knapp, B. G., Rottman, G., et al. (2004). A composite Mg II index spanning from 1978 to 2003. *Space Weather*, *2*, S10005. https://doi.org/10.1029/2004SW000084

von Storch, H., & Zwiers, F. W. (1999). *Statistical analysis in climate research*. Cambridge, UK: Cambridge University Press.

Wang, Y.-M., Lean, J. L., & Sheeley, N. R. Jr. (2005). Modeling the Sun's magnetic field and irradiance since 1713. *The Astrophysical Journal*, *625*(1), 522–538. https://doi.org/10.1086/429689

Wilks, D. S. (1995). *Statistical methods in the atmospheric sciences*. San Diego, CA: Academic Press.

Willmott, C. J., & Matsuura, K. (2005). Advantages of the mean absolute error (MAE) over the root mean square error (RMSE) in assessing average model performance. *Climate Research*, *30*, 79–82. https://doi.org/10.3354/cr030079

Willson, R. C. (2014). ACRIM3 and the total solar irradiance database. *Astrophysics and Space Science*, *352*(2), 341–352. https://doi.org/10.1007/s10509-014-1961-4

Woods, T. N., Chamberlin, P. C., Harder, J. W., Hock, R. A., Snow, M., Eparvier, F. G., et al. (2009). Solar Irradiance Reference Spectra (SIRS) for the 2008 Whole Heliosphere Interval (WHI). *Geophysical Research Letters*, *36*, L01101. https://doi.org/10.1029/2008GL036373

Woods, T. N., Eparvier, F. G., Harder, J., & Snow, M. (2018). Decoupling solar variability and instrument trends using the Multiple Same-Irradiance-Level (MuSIL) analysis technique. *Solar Physics*, *293*(5), 76–96. https://doi.org/10.1007/s11207-018-1294-5

Woods, T. N., Prinz, D. K., Rottman, G. J., London, J., Crane, P. C., Cebula, R. P., et al. (1996). Validation of the UARS solar ultraviolet irradiances: Comparison with the ATLAS 1 and 2 measurements. *Journal of Geophysical Research*, *101*(D6), 9541–9569. https://doi.org/10.1029/96JD00225

Woods, T. N., Tobiska, W. K., Rottman, G. J., & Worden, J. R. (2000). Improved solar Lyman α irradiance modeling from 1947 through 1999 based on UARS observations. *Journal of Geophysical Research*, *105*, 27,195–27,215. https://doi.org/10.1029/2000JA000051

Yeo, K. L., Krivova, N. A., & Solanki, S. K. (2017). EMPIRE: A robust empirical reconstruction of solar irradiance variability. *Journal of Geophysical Research: Space Physics*, *122*, 3888–3914. https://doi.org/10.1002/2016JA023733